Microwave Manipulation of Atoms on a Chip

by

David C. McKay

A THESIS SUBMITTED IN PARTIAL FULFILLMENT OF THE
REQUIREMENTS FOR THE DEGREE OF BACHELOR OF APPLIED SCIENCE

DIVISION OF ENGINEERING SCIENCE

FACULTY OF APPLIED SCIENCE AND ENGINEERING

UNIVERSITY OF TORONTO

Supervisor: J.H. Thywissen
Department of Physics

April 13, 2006

Abstract

The goal of the Ultracold Atoms Lab at the University of Toronto, under the supervision of Professor Joseph Thywissen, is to perform experiments with a Fermi/Bose mixture of ^{40}K and ^{87}Rb in a micromagnetic chip trap. ^{40}K and ^{87}Rb have internal hyperfine states that are separated by frequencies of 1.3 GHz and 6.8 GHz respectively. In order to attain the greatest control over these atoms, tools must be constructed to manipulate their internal states. This thesis details work done towards creating those tools and ultimately manipulating ^{40}K and ^{87}Rb in a micromagnetic chip trap. Microwave frequency generators were built and tested at 1.3 and 6.8 GHz. First tests showed ^{40}K atoms ejected from the chip trap using this source. To more efficiently couple these microwaves into the vacuum system, a new apparatus for holding the chip trap (the 'stack') was designed and constructed. Because the vacuum compatibility of the new stack is unknown, a new vacuum system was built to test the vacuum properties of materials using a magneto-optical atom trap as an ultrasensative pressure gauge. Data is presented from this magneto-optical pressure gauge which demonstrates the gauges ability to measure changes in the system pressure. This thesis provides the tools necessary to test new materials for ultra high vacuum compatibility and lays the foundation for microwave manipulation of ^{40}K and ^{87}Rb .

Acknowledgments

First, I would like to thank everyone in the lab, Seth, Stefan, Marcius, Lindsay and Alan for all their help and support. Without them none of this would be possible. Obviously I would like to thank Professor Joseph Thywissen for supervising this thesis and for being an excellent mentor over the past two years. I will forever be indebted to him for giving me my first real taste of research. Finally, I must thank Jessie Newton for putting up with my late nights at the lab.

I would like to acknowledge financial support for some of this project from the National Science and Engineering Research Council (NSERC) of Canada.

Preface

At the time that I wrote this thesis, it was two years ago that I started working in the Ultra Cold Atoms Lab headed by Joseph Thywissen. I had received an NSERC grant to do summer research in the physics department at the University of Toronto. I wanted to try research out because I had worked the summer before as a software developer and the work was, kindly, less than simulating. Once we received an NSERC grant, it was the students job to pick a project from a list on the physics website. That semester was my first taste of quantum physics and I found it quite interesting. Joseph's work was appealing and before I knew it I was starting the summer in his lab. By the end of the summer, after having successfully constructed a working Potassium 40 dispenser, I was hooked on the idea of research. I felt that I fit in well in the lab and I enjoyed working with Joseph as a supervisor. When the next summer rolled around, once again I found myself in MP023 for another summer of physics in the Ultra Cold Atoms Lab. By this time I had also committed myself to a thesis with Joseph the following school year and I was ready to get going on a long term project.

Initially, we discussed constructing microwave resonators on the chip. However, we realized that this meant two things. First, we would need to get a source of microwaves. Second, we would need to construct a new apparatus for holding the chip (the 'stack') because the idea of coupling microwaves into the system was not a part of the original design. While I was constructing these, I was going to think about various ways we could put antennae and resonators onto the chip. The summer had a plan and I set out to complete these tasks. First, I finished off the 1.3 GHz source that Ian Leroux had designed, but not constructed for his thesis the year before. I

spent some time playing around with stub tuning the microwave signal into the vacuum system, with some success. Reflections from the vacuum were below 10% and we briefly played with microwave evaporation. However, there was little time to play with new techniques because bigger things were brewing around the lab. The march towards Fermi Degeneracy on a chip was on. Therefore, I proclaimed the 1.3 GHz source built and moved on to the next task.

At this point I turned my attention fully towards constructing a new apparatus to hold the chip in the vacuum system. This also meant changing the flanges for the vacuum system, so I also investigated new methods to couple microwaves into the system. Several products already existed on the market, such as SMA feedthroughs and in-vacuum coaxial cable, so I ordered these and moved on to designing the stack itself. After several weeks of playing in CAD, I had what I felt was an elegant replacement to the existing stack. Because the new stack had many contacts placed so close together, it was hard to design a system that could be feasibly machined. Also, some work went into considering the possible ways to connect to the chip. However, a solution was conceived and off the plans went to the shop to get made into the new Thywissen group stack.

With the stack out of my hands, I started planning for the construction of the second microwave source at 6.8 GHz. By this time, the summer was coming to a close and the school year, and the thesis, were approaching. It had been a very good summer, not just personally, but for the lab. We had achieved Fermi Degeneracy on a chip thanks to the hard work of the members of the lab. It was exciting to be a part of something new in physics and I was happy to be but a small part. With this backdrop, Joseph and I began discussing ideas for my thesis. In retrospect, they were lofty goals, but I feel it is better to try for the impossible and see how far you can get. Slowly we settled on the idea of probing spin mixtures of Potassium-40. However, the first part of the project would be to get the high frequency sources and the stack fully functional and into the main system.

I continued to work on the high frequency stuff throughout the fall and by November the 6.8 GHz source had been fully built and tested. It was becoming time to move the stack into the main system, but we had become increasingly leery about the different materials the new stack was being constructed of, specifically anodized aluminum. Seth suggested that we test the vacuum compatibility of these materials by constructing a new system with a MOT. According to him, it would be easy because we had an old glass cell and I could just use the lasers from the main experiment which were already amplified and locked. And so I set off to make a new vacuum system, a MOT and test the vacuum properties of the stack.

Despite our earlier goals, building the new vacuum and setting up the MOT took me the rest of the school year. We never even got a chance to test the stack because we did not put it into the vacuum system this first time around. The idea was to use these measurements as a control group for comparison when we do put the stack in later on. Although this project only got a fraction of the way I would have liked, it was a learning experience better than I could have every asked for. Designing, ordering and building a vacuum system, baking it and leak testing it is something that will be forever useful. Also, I got my first real experience with optics and learned some things that will definitely help me in the future. Often, I am told, this is the way research goes. It is never as you had planned, but you get somewhere positive in the end. That has certainly been my experience, one I will always cherish.

In this document I have outlined some of the basic theory behind the atomic cooling that we do in the Ultra Cold Atoms Lab. There is a strong focus on Magneto-Optical Trapping and Evaporative Cooling, since these areas directly related to the work I have done. After discussing some theory, I go on to discuss the work I did on completing both of the high frequency sources. This leads into the section of the design and construction of the new stack. Finally, I discuss the new vacuum system and MOT I built for testing the stack and I present some initial data regarding the

MOT lifetime in that system. The focus is always the eventual goal of manipulating the atoms in a chip trap. To that end, there is still work to be done testing the stack and then assembling it in the main experimental system. Hopefully, this work will be completed in summer 2006.

Contents

List of Figures

List of Tables

Chapter 1

Introduction

Over the course of the past two decades, cold atoms have evolved into one of the most exciting areas of physics research. Low temperature physics has always brought a rich variety of new phenomena into the world such as superfluidity and superconductivity. However, traditional low temperature physics relied on the use of liquid Helium and dilution refrigerators. When laser cooling was developed in the early eighties it ushered in a whole new era of low temperature physics of dilute atomic gases. The late eighties brought the innovation of the magneto-optical trap, which allowed for large numbers of very cold localized atoms for cold atom experiments. This brought a number of new discoveries, but none as significant as Bose-Einstein Condensation (BEC) of rubidium and then sodium in 1995. Although the concept of BEC had been observed in superfliud helium, the setup of trapped, dilute atomic gases allowed for complete control of the system. Later, in 1999, a system of fermions, ^{40}K , was brought down below the Fermi Temperature. This was significant because most condensed matter systems consist of fermions (electrons) in a degenerate state.

The goal of cold atom experiments is to get the most precise control over the system as possible. One such way to increase that control is through the magnetic fields in which the atoms are trapped. The most precise control of the fields is through the use of lithography techniques on a suitable substrate, often known as chip traps[4]. These wires can be made into complex patterns for a variety of applications includ-

ing atomic waveguides and beam splitters. However, they can even improve more standard experiments by increasing the evaporation times since chip wires can provide more tighter atomic confinement. One of the first chip traps was demonstrated by Reichel, Hansel and Hansch[5], which used a U-trap loaded from a MOT created above the surface of the chip by bouncing the laser beams off the chip surface.

Because of faster evaporation times, chip traps place less stringent demands on the vacuum pressure of the system and lead to simpler, single chamber experiments. The goal of the Thywissen Ultra Cold Lab at the University of Toronto is to realize these benefits with a chip trap to simultaneously get Bose and Fermi degeneracy with ^{87}Rb and ^{40}K . So far, the lab has been very successful in this endeavor and has reached the stated goal[6]. However, in the spirit of atomic physics we would like to control the atom as much as possible. Part of the internal state structure of most atoms is the hyperfine energy splitting due to the interaction of the magnetic moment of the electrons with the magnetic moment of the nucleus. This results in an energy level splitting of 1.3 GHz for ^{40}K and 6.8 GHz for ^{87}Rb between two hyperfine levels in the $^2S_{1/2}$ ground state. Being able to control transitions between these levels would allow for many interesting applications, such as creating mixtures of the different spin states and evaporating using these microwave transitions.

However, the lab does not currently have the ability to control transitions between these states. In the following, we present results towards the manipulation of these states in our experiment. First, we discuss the construction of the source of these microwaves using a frequency multiplied signal from a direct digital synthesizer. Once the source has been constructed we need a way to couple those microwaves into the system. Therefore, we next discuss the construction of a new apparatus to hold the chip in the vacuum, which has been designed to couple microwaves all the way to the chip surface. Finally, we discuss a setup for testing the vacuum compatibility of materials that we plan on using for the new chip 'stack'. When all the testing is complete, the system will be ready to go into the main experiment. This will allow us

to couple microwaves to the chip and have ultimate control over hyperfine transitions of ^{40}K and ^{87}Rb .

Chapter 2

Cooling Atoms

To give an appropriate context for the work performed in this thesis, it is necessary to review the basic principles developed over the past two decades for trapping and cooling atoms. Taking atoms from a room temperature vapour and creating a cloud with a temperature in the nano-Kelvin range has been a large accomplishment of atomic physics. Today, the process has been repeated a sufficient number of times for one to talk of a general procedure for the cooling and trapping of alkali atoms. Figure 2.1 shows the basic steps involved in the cooling process and the temperatures at each of these stages.

2.1 Phase Space

An important concept in statistical mechanics is that of the phase space density ($\rho(\vec{r},\vec{p},t)$), which is the probability density for a particle to be at the location $\vec{r}$ with momentum $\vec{p}$[7]. The goal of cooling atoms is not necessarily to reduce the temperature, which is related to momentum, but to increase the phase space density at $\vec{r}=0$,$\vec{p}=0$. This is because interesting phenomena such as Bose-Einstein Condensation (BEC) and Fermi Degeneracy require high phase space densities, not low temperatures. However, to achieve phase space densities required to observe these phenomena with reasonable spatial densities, low temperatures are important. The concept of phase space density is semi-classical as it implies that we know the position and momentum of a particle

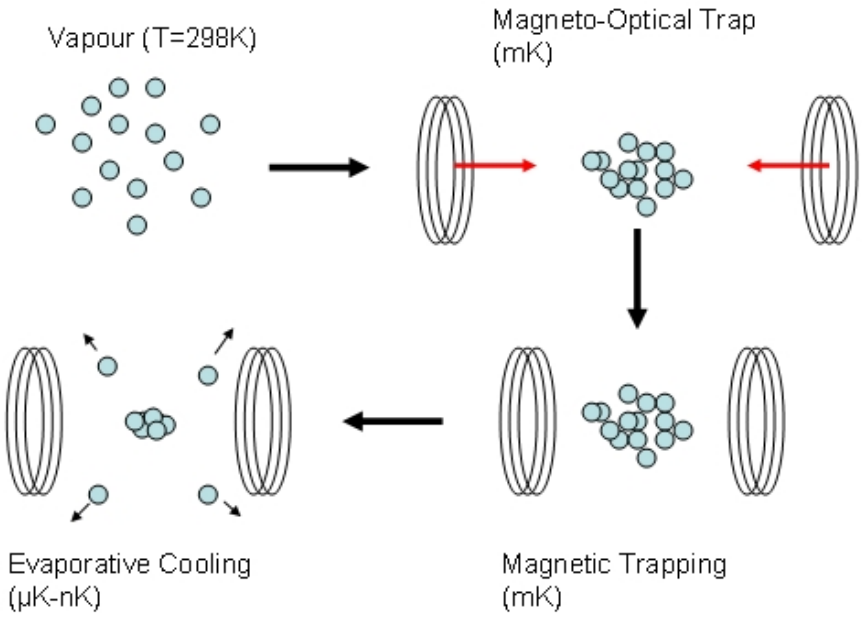

Figure 2.1: Typical process for cooling atoms with the temperature of the cloud labeled at each step.

exactly. Therefore, as quantum behaviour becomes observable the fugacity ($e^{\mu/kT}$) is used for fermionic atoms and the ground state occupation is used for bosonic atoms[6].

An important concept that will become relevant in the following discussion of cooling techniques is Louiville's Theorem[8]. While a proof can be found in the literature, the result is that for a system governed by Hamiltonian mechanics, phase space density cannot increase. A qualitative argument for this principle can be given for a system in a harmonic trap. If one increases the trap frequency (tightens the confinement of the trap), spatial density will increase. However, this will increase the energy of the particles in the trap and therefore decrease the momentum density. Overall, phase space density will not be affected.

2.2 Laser Cooling

The first process in cooling atoms to quantum degeneracy is the process of laser cooling. A simple entropic argument may be given for laser cooling, in that thermodynamically a laser is at a low temperature since it has a low entropy[9]. When a laser photon (of low entropy) is absorbed by an atom and spontaneously re-emitted at higher entropy heat flows given by the formula $\Delta S = \dot{q}/T$.

For a more detailed analysis of laser cooling, we must analyze the specific processes involved in the laser-atom interaction. When a laser beam is incident on an atom in the ground state there is some probability that the atom will absorb a photon from the beam. If we let the beam have a wavenumber, k, then the absorption imparts a momentum kick $\hbar k$ in the direction of the beam propagation. Once in the excited state the atom has a probability of spontaneously emitting the photon in a random direction. Integrating over these directions, the average momentum kick imparted on the atom through spontaneous emission is 0. Overall, the atom has been given a momentum $\hbar k$ in the direction of the beam. There is also a probability of stimulated emission. This causes the atom to emit a photon in the direction of the beam propagation which gives a momentum kick of $-\hbar k$. Overall, the momentum of the atom is not changed.

The next step is to use the process of absorption and spontaneous emission to slow the atom. We want the atom to absorb photons when it moves counter to the beam propagation and not absorb when it is moving with the beam. This situation is achieved when two counter-propagating beams are set at a frequency slightly lower than the frequency separating two internal states of the atom. This is known as red-detuning the beams. From classical mechanics we know that the change in frequency of light from a source moving with velocity v (the Doppler shift) is:

$$\Delta\omega = kv \tag{2.1}$$

In the following discussion, we consider an idealized two-state atom where the two levels are separated by energy $\hbar\omega_a$. As mentioned above, when the atom is in the excited state ($|e\rangle$), there is some probability of spontaneous decay. The lifetime of the state, τ is given by $1/\Gamma$ where Γ is known as the linewidth of the atomic transition. Using the density matrix formalism, the probability that an idealized two level atom will be in the excited state is[7],

$$\frac{s}{2(1+s)} \tag{2.2}$$

where s is the saturation parameter given by,

$$s = \frac{\frac{\Omega^2}{2}}{\delta^2 + (\frac{\Gamma}{2})^2} \tag{2.3}$$

where $\delta = \omega_l - \omega_a$ in the atomic rest frame and Ω is the Rabi frequency. The Rabi frequency characterizes how strongly the field couples the ground and excited states together. When $\delta = 0$, $s = s_0$, which is the on-resonance saturation parameter. If in the lab frame the atom moves towards the laser beam, then in the rest frame of the atom the laser beam is moving towards the atom. Therefore by equation 2.1, the laser frequency is increased. In the opposite case of an atom moving away from the beam, the frequency is decreased. From equation 2.2, we see that the absorption is peaked at ω_a, the frequency separating the internal states of the atom. Since the beams are red-detuned from that frequency, the atom moving towards the laser beam absorbs more of the light than the atom moving away from the beam. The result is that the atom slows down as illustrated in figure 2.2.

The atom cooling force is [10][7]:

$$\vec{F} = \frac{\hbar \vec{k_L} \Gamma}{2} \frac{s}{1+s} \tag{2.4}$$

The velocity enters into equation 2.4 since s is velocity dependent. In the low velocity limit:

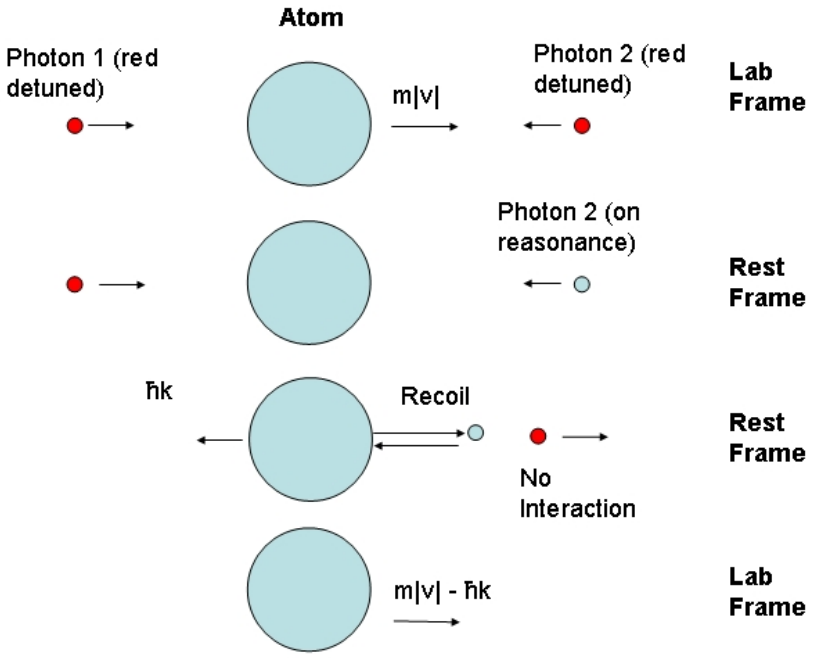

Figure 2.2: Schematic representation of laser cooling in one dimension

$$\vec{F}(\vec{v}) = \frac{8\hbar k^2 \Delta s_0 \vec{v}}{\Gamma(1 + s_0 + \left(\frac{2\Delta}{\Gamma}\right)^2)^2} = -\beta\vec{v} \tag{2.5}$$

where the Δ in equation 2.5 refers to $\omega_l - \omega_a$ in the lab frame. Because the force is proportional to velocity the system cannot be described by Hamiltonian mechanics. Therefore, laser cooling results in phase-space increase. This equation implies that $\vec{v}$ will damp to 0, which is not true and in practice the limit of Doppler laser cooling is the Doppler temperature $(\hbar\Gamma)/(2k_B)$.

2.3 Magneto-Optical Trap

Although laser cooling is a good process for cooling atoms from room temperature to the mK range, all it provides is a velocity dependent force. Instead of bringing the laser into resonance as the atoms move towards it, we need the atom to move into resonance as it moves from the centre of a fixed location in space. A method for trapping the atoms using this principle was first demonstrated in 1987[11]. Using a

set of anti-Helmholtz coils, a magnetic field zero is created in vacuum. In each of the 3 orthogonal directions the field goes linearly through the center. Because of the $\vec{L}\cdot\vec{B}$ and $\vec{S}\cdot\vec{B}$ perturbations to the Hamiltonian, there is a Zeeman shift of the energy levels proportional to the magnetic field. Consider the case where the transitions is between a state F=0 to F=1. In the F=1 state the levels (m_F=-1,m_F=0,m_F=1) will all split in the field. In the region of negative B field, the state m_F=1 will lower in energy. Therefore, the transition F=0,m_F=0 $\longrightarrow$ F=1,m_F=1 is brought closer to resonance. The opposite applies for the region of positive field where the transition F=0,m_F=0 $\longrightarrow$ F=1,m_F=-1 is brought closer to resonance. Therefore, we set up two counter-propagating, red-detuned beams. As the atom moves from the magnetic field zero into a region of higher field, it is brought into resonance and pushed back to the field center. However, the atom will absorb photons from both beams and no trapping will occur. To prevent this from happening, we use selection rules for atomic transitions. If we have σ^+ light the transitions $\Delta m_F = -1$ is forbidden and if we have σ^- light the transitions $\Delta m_F = 1$ is forbidden. Therefore, one of the beams is σ^+ and the other is σ^-, arranged in such a way that the force of the light on the atom is always back towards the trap center (see figure 2.3).Because the magneto-optical trap works with red-detuned light, the atoms are initially laser cooled before they get caught in the trap.

Quantitatively, the force that the atom experiences is similar to the force caused by the resonance induced by the atomic Doppler shift. Instead, with the MOT the shift is provided by $\mu_B/\hbar\frac{\partial B}{\partial z}z$ [10]. Therefore the total force on the atom moving in the positive z direction is[10]

$$\vec{F} = -\frac{\hbar k}{2}\Gamma\frac{(\Omega/2)^2}{\left(\Delta + kv_z + \frac{\mu_B}{\hbar}\frac{\partial B}{\partial z}z\right)^2 + \Omega^2/2 + (\frac{\Gamma}{2})^2}, \tag{2.6}$$

where if Δ and $\frac{\partial B}{\partial z}$ are negative the force cools and traps. For small velocities and

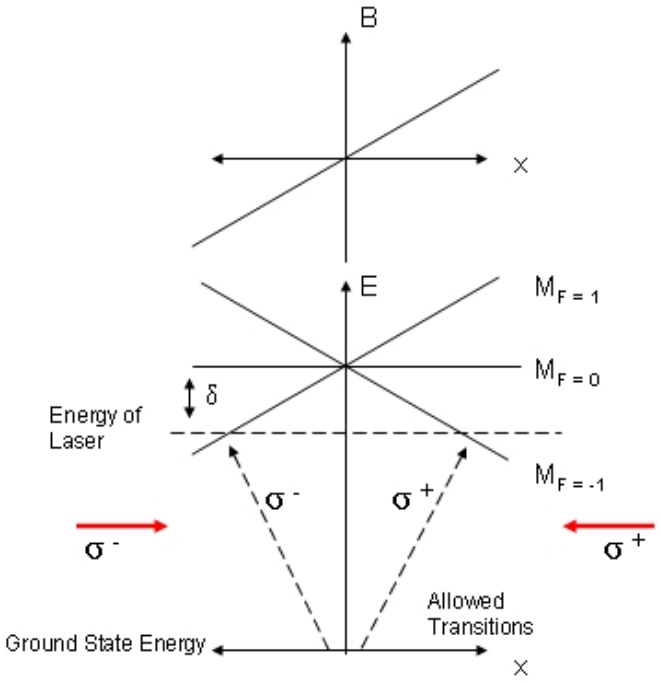

Figure 2.3: The process of magneto-optical trapping

displacements, the force is proportional to the velocity and displacement,

$$\vec{F} = -\alpha z - \beta \dot{z}. \tag{2.7}$$

This is a damped, simple harmonic oscillator. However, the trap is not nearly as perfect as portrayed by the above relations. For this study, we are quantitatively interested in the effect of certain parameters on the number of atoms contained in the trap. We model the trap using the formula[12]

$$\frac{dn}{dt} = A - Bn - Cn^2, \tag{2.8}$$

where A is the loading rate, B is the loss related to the background pressure in the system and C is the loss from collisions inside the trap. Collisional loss has been observed to dominate over background losses[12]. The main collisional loss which dictates the value of C is that of excited state collisions[13]. Since the goal of the experiment is to measure the background pressure, we will let C $\longrightarrow$ 0. However, we

must consider it as a factor when analyzing data of n vs. t in later sections. If C = 0 then

$$\frac{dn}{dt} = A - \frac{n}{\tau}, \tag{2.9}$$

$$n(t) = n_o(1 - e^{-t/\tau}). \tag{2.10}$$

The loading rate, A, has an analytical form given by[14]

$$A = \frac{1}{2} n V^{\frac{2}{3}} v_c^4 \left(\frac{m}{2kT}\right)^{\frac{3}{2}}, \tag{2.11}$$

where V is the trapping volume and v_c is the trapping velocity. The τ from collisions between the trapping element y and a background element x given by[14][15]

$$\frac{1}{\tau} = n_x \sigma_{x-y} \left(\frac{3kT}{m_x}\right)^{\frac{1}{2}}, \tag{2.12}$$

If the background pressure of the system is dominated by a certain element, then the lifetime of the MOT can be used as a pressure gauge. A complication to this idea is the fact that to make a MOT, one usually loads a high vapour pressure of the trapping element into the chamber. The lifetime will then be a measure of this pressure, not the usual background pressure of the system. Therefore, to be an effective pressure gauge, the MOT needs to be run with a low partial pressure of the trapping element, which will unfortunately lead to a smaller MOT. While it is not easy to determine if the partial pressure of the loading element is very low, it is easy to determine if the loading element's partial pressure is dominating the system. For example, if we suppose that $n_y >> n_x$ then

$$\frac{1}{\tau} = n_y \sigma_{y-y} \left(\frac{3kT}{m_x}\right)^{\frac{1}{2}}, \tag{2.13}$$

$$n(\infty) = A\tau, \tag{2.14}$$

$$= \frac{1}{2} V^{\frac{2}{3}} v_c^4 \sigma_{y-y}^{-1} \left(\frac{m}{kT}\right)^2 12^{-\frac{1}{2}}. \tag{2.15}$$

Therefore, the final atom number is independent of the vapour pressure in the cell. This result can be used to determine if the loading element has a partial pressure much greater than the background gas.

2.4 Evaporative Cooling

While the magneto-optical trap is a very robust and essential tool for reaching high phase space densities, it cannot reach the limit of a dilute alkali condensate. The ultimate phase space density attainable using light is limited by rescattering and scattering[16]. However, the cloud is cool enough to be transferred into a magnetic trap. Once in a magnetic trap, the hottest atoms can be selectively removed in a process known as evaporation.

2.4.1 Magnetic Trap

Earnshaw's theorem prevents an electrostatic field from trapping a magnetic monopole or electric charge[7]. Essentially this derives from Maxwell's equation, which dictates that $\vec{\nabla} \cdot \vec{E} = \vec{\nabla} \cdot \vec{B} = 0$. Therefore, it is impossible to create a true minimum of $\vec{B}$, however, it is possible to create a minimum of $|\vec{B}|$. The potential energy of a magnetic moment, $\vec{\mu}$ in a field, $\vec{B}$ is $-\vec{\mu} \cdot \vec{B}$. If the magnetic moment will follow the field, then

$$U = -g_F \frac{\mu_B}{\hbar} m_F |\vec{B}|, \tag{2.16}$$

where m_F is the projection of the atomic angular momentum onto the B axis. This energy is the Zeeman shift of the atomic sublevels. Since we can make $|\vec{B}|$ be a minimum, then we can make a trap. Practically, it is difficult to make magnetic traps with depths greater than 1K. Also, the atom has to move slowly enough through the trap that the magnetic moment adiabatically follows the magnetic field. A spherical quadrupole trap has the problem that the magnetic field minimum is zero. When very cold atoms go through the center, they lose their quantization axis, rotate their magnetic moment and become untrapped. Trap geometries such as the Ioffe-Pritchard

trap correct this problem.

2.4.2 Evaporating

Once the atoms are in a magnetic trap, evaporative cooling can take place. Qualitatively, the idea of evaporative cooling is simple. Remove the hottest atoms from the trap and allow the atoms to rethermalize through collisions. Since the average energy per atom has decreased, the gas will rethermalize to a lower temperature. This process cannot be described with Hamiltonian mechanics and therefore can increase phase-space density.

Two Level Transitions

For evaporative cooling to work we need a method to selectively remove the hottest atoms from the trap. Classically we know that in a trap, the most energetic particles can travel the furthest from the trap center before they lose all their kinetic energy. If there were a way to make the trap reverse itself a certain distance from the center then all the atoms above a certain energy would be ejected. Such a method does exist with atoms in a magnetic trap, but first we need to discuss the theory of the interaction between an atom and a weak electromagnetic field. The Hamiltonian for such an interaction is given by

$$\hat{H}_{int} = -\hat{\mu} \cdot \vec{B}, \tag{2.17}$$

$$\hat{H}_{int} = 2\mu_B \hat{S}_z B_0 cos(\omega t). \tag{2.18}$$

If we consider just a two state atom ($|1\rangle$,$|2\rangle$) separated by energy $\hbar\omega_a$ then solving the time-dependent Schrodinger equation we get [7]

$$|\langle\Psi|1\rangle|^2 = \cos^2\left(\sqrt{\Omega^2+\Delta^2}t/2\right) + \frac{\Delta^2}{\Omega^2+\Delta^2}\sin^2\left(\sqrt{\Omega^2+\Delta^2}t/2\right), \tag{2.19}$$

$$|\langle\Psi|2\rangle|^2 = \frac{\Omega^2}{\Omega^2+\Delta^2}\sin^2\left(\sqrt{\Omega^2+\Delta^2}t/2\right), \tag{2.20}$$

where $\Delta = \omega - \omega_a$ and where Ω is the Rabi frequency defined by

$$\Omega = \frac{2\mu_B B_0}{\hbar}\langle 1|\hat{S}_z|2\rangle. \tag{2.21}$$

Therefore, when the field oscillates at the same frequency as an atomic transition, the atom oscillates between states $|1\rangle$ and $|2\rangle$. If $|1\rangle$ is a trapped state and $|2\rangle$ is an untrapped state, the field will eject the atom from the trap. However, we still need a way to only eject the hottest atoms. If we use two magnetic sublevels such as $m_F = 1/2$ and $m_F = -1/2$ as the two states, then from the Zeeman shift (equation 2.16) the resonance between these states changes with position. If we set the frequency of the source to the separation of these states at a certain distance from the trap center, only atoms that reach that distance will be ejected. This process is illustrated in figure 2.4.

Typically evaporation is done using radio frequency fields and making transitions between different magnetic sublevels in the same hyperfine level. Often, such as in the ^{87}Rb F=2 state, several transition have to occur before the atom reaches an untrapped state. This makes the theory more complicated than the two state assumption, however, the idea remains the same. Also, evaporation can occur between magnetic sublevels in different hyperfine levels. In this case the frequency of the field is in the microwave regime (>1 GHz). To actual perform evaporative cooling using these fields, the frequency is set to above the trap depth and swept down in frequency to remove more and more atoms. The speed of sweep is determined by the rethermalization time of the atoms, which is a function of the collisional cross-section and the trap confinement.

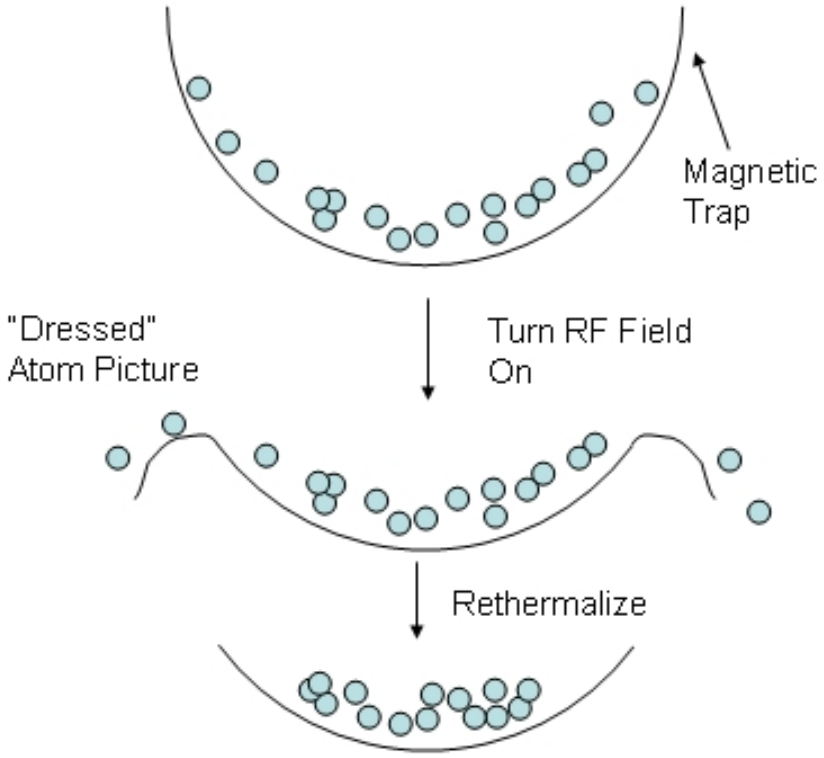

Figure 2.4: The process of evaporative cooling

Chapter 3

Hyperfine Manipulation of ^{40}K and ^{87}Rb

Both ^{40}K and ^{87}Rb have a ground state that is split into two hyperfine states separated by 1.3 and 6.8 GHz respectively. There are many reasons for wanting to create transitions between these two states. The most obvious reason is for evaporative cooling (see section 2.4). In a two-species gas, the Zeeman splitting between the two species is similar. It can become difficult using radio frequencies to remove one species from the trap without affecting the other. The hyperfine transitions allow precise control over the two different species given the large difference in the frequencies. Another reason is for preparing arbitrary states. In the ground state, the atom has many different magnetic sublevels, corresponding to the orientation of the atomic angular momentum. Transitions between these states using the Zeeman splitting is not precise because each level is split by the same amount. Conversely, hyperfine transitions allow one to go to a specific m_F level. This can be useful for creating interesting spin mixtures. In the end, the ability to manipulate the hyperfine levels of ^{40}K and ^{87}Rb is just another useful tool for the atomic physicist to control the internal atomic states.

3.1 Atomic Structure of ^{40}K and ^{87}Rb

Since ^{40}K and ^{87}Rb are both alkali-metal atoms, their internal states are similar. All alkali atoms have one valence electron and the rest of the states are in closed shells. Therefore, the spin, orbital and total electronic angular momentum are all dictated by the single outer electron. In the ground state, the electron has an orbital angular momentum of 0 and is therefore in the $^2S_{1/2}$ (S=1/2,L=0,J=1/2). There is a perturbation to the energy $\hat{J} \cdot \hat{I}$ where $\hat{I}$ is the angular momentum operator of the nucleus. This perturbation causes a splitting that gives rise to the hyperfine structure of the atom. With this perturbation, the Hamiltonian is diagonalizable in the $\hat{F} = \hat{J} + \hat{I}$ basis. In $^2S_{1/2}$ there are two values of F, F=I-1/2 and F = I + 1/2. Each of these states is further split into magnetic sublevels corresponding to the orientation of F. In field-free space, these 2F+1 levels are degenerate.

The value of I for ^{40}K is 4 and for ^{87}Rb is 3/2. Therefore, ^{40}K is split in F = 9/2,7/2 and ^{87}Rb is split into F = 1,2. The energy separation between these states for ^{40}K is 1.3 GHz and for ^{87}Rb is 6.8 GHz. When calculating the effect of the magnetic field on each one of these states we get equation 2.16. For ^{40}K g_F is 2/9 for F=9/2 and $-2/9$ for F=7/2. For ^{87}Rb g_F is 1/2 for F=2 and $-1/2$ for F=1 [17]. A final note about the hyperfine states is that they have no natural linewidth [9]. There is no spontaneous decay between the hyperfine states. Figure 3.1 illustrates the ground and excited state levels of ^{40}K and ^{87}Rb . In atomic physics the transition between the ground state $^2S_{1/2}$ and the first excited state $^2P_{1/2}$ is known as the D1 transition and the transition between the ground state $^2S_{1/2}$ and the second excited state $^2P_{3/2}$ is known as the D2 transition.

3.2 Building Microwave Sources

From the previous section, we know that ^{40}K and ^{87}Rb have hyperfine states separated by microwave frequencies. The next step is to design a microwave source to

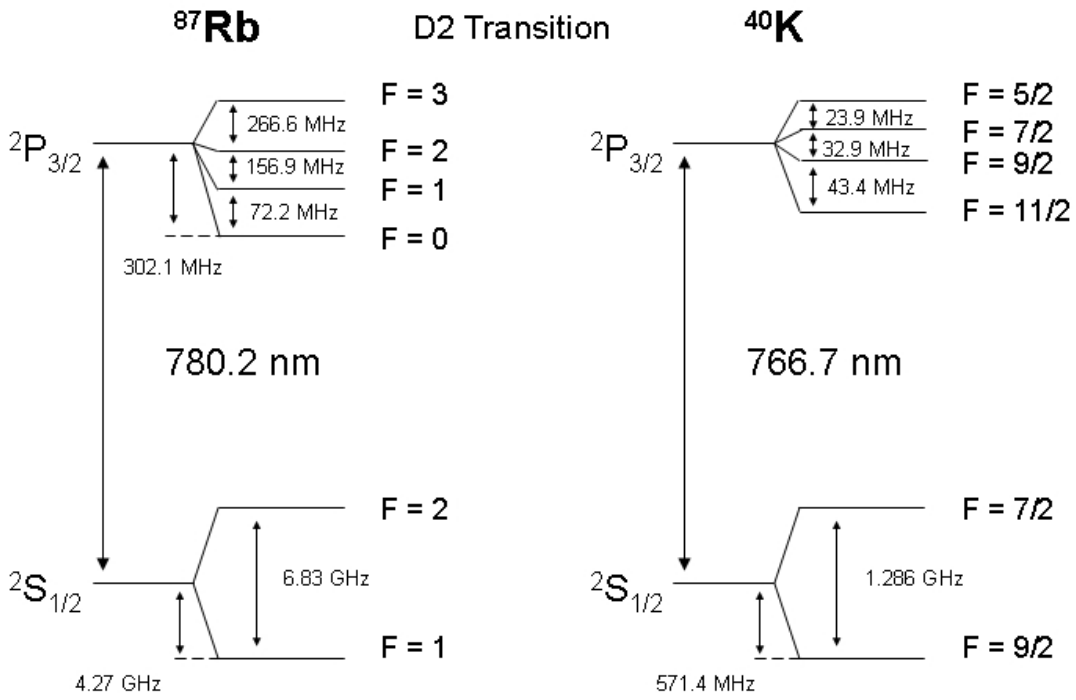

Figure 3.1: Atomic levels of ^{40}K and ^{87}Rb [1][2]

manipulate these states. The following details the work done in the Thywissen lab towards building such a source.

3.2.1 Requirements

Before designing this source we need to understand its requirements. The original intent of these sources was to evaporatively cool a dual species gas of ^{40}K and ^{87}Rb . The requirements of evaporative cooling are:

- Frequency: Atoms are only ejected from the trap if they are resonant with the atomic transition between the trapped and untrapped state. In field-free space the hyperfine transitions are 1.3 and 6.8 GHz. Therefore, the center frequency of the source should be near those frequencies.

- Tunable: As illustrated in section 2.4 the separation between trapped and untrapped states changes with the increase in the magnetic field. Therefore, to perform evaporative cooling we need to be able to tune the frequency around

1.3 and 6.8 GHz. The magnetic trap in our experiment is ∼200 G/cm and the trap size is less than 1 mm in size. At the maximum trap size the field is ∼20G. From equation 2.16 the frequency shift is $g_F m_F \times 1.43$ MHz/G. For ^{40}K this corresponds to a maximum frequency shift of ∼50MHz and for ^{87}Rb ∼40MHz. Therefore, the source should be tunable ±50MHz around the center frequency.

- Stability: The source must be stable in two ways. First, it must be stable on a short time scale or else the evaporation will not be effective and/or too many atoms will be evaporated. Second, it must be stable on a long time scale or else the experiment will need to be recalibrated on a periodic basis.

- Speed: For our experiment the evaporation cycle occurs from 30MHz to 3MHz in 3 seconds[6]. The source must be able to sweep through this frequency range in this time in a stable manner.

- Resolution: We must be able to specify the frequency to within 10 Hz.

- Noise: The source should not have any harmonic noise that will cause unwanted atomic transitions. For example, the 6.8 GHz should not have any 1.3 GHz noise, so that it can act independently on the ^{87}Rb .

3.2.2 Possible Designs

There are many different ways to build a microwave source. The easiest method is to purchase a commercial synthesizer, however, they are expensive ($50,000) and they still have a tough time with the fast switching times required. Because our source does not require a large operating range, there are several less expensive and ultimately better solutions available.

Mixing

While it is expensive to buy a high frequency synthesizer, it is less expensive to buy a stable high frequency source locked to one frequency. To provide the required

tunability, the signal would be mixed with a radio frequency synthesizer, which could be easily obtained.

Frequency Multiplication

This design takes a low frequency synthesizer and multiplies it up to the microwave range. While this method is inexpensive, it could introduce a lot of harmonics into the system and it also multiplies any noise in the original source.

Frequency Division

High frequency voltage controlled oscillators (VCOs) are readily available, however, they lack precision control and stability. Fortunately, there exists techniques to lock VCOs to more stable sources. Therefore, we can divide down the signal from the high frequency oscillator and lock it to a less expensive, stable low frequency synthesizer.

3.2.3 The Design

The design we selected for constructing both the 1.3 GHz and 6.8 GHz sources is to use a low frequency source and multiply it up to the final microwave frequency. There are three main reasons for this decision:

- Robust Low Frequency Source: The direct digital synthesizer (DDS), which will be described in detail in the following section, is a product from Analog Devices capable of creating signals up to 500 MHz. It has all the proper features; stability, 0.1 Hz resolution, inexpensive (<$400) and fast (built in linear ramp).
- Simplicity: With the low frequency source, it is very easy to multiply the signal up with a few off the shelf components. Multiplying eliminates the need for a high frequency oscillator, which would complicate the setup.
- Cost: The high frequency source not only adds complexity, but also significant cost. Each high frequency oscillator costs on the order of $1000 without reducing other costs.

This design can be broken into four distinct parts. The first is the low frequency source, in this case the AD9858 from Analog Devices. Next is the frequency multiplication, which takes the low frequency signal and converts it into a high frequency signal. To facilitate the frequency multiplication the other parts of the system are filters and amplifiers. Filters remove unwanted signals created by the nonlinear multipliers. The amplifiers rebuild the signal power after most of it is lost in the multiplication process. All of these components are described below with their figures of merit.

AD9858 - Direct Digital Synthesizer

The main component of our design is the direct digital synthesizer (DDS) from Analog Devices. Essentially, the DDS is a lookup table with a fast digital to analog converter. The effect is a sinusoid in discrete voltage steps. With appropriate filtering, this signal can be made into a clean sinusoid. The timing for the chip is based on an external voltage controlled oscillator (VCO). The maximum frequency of the AD9858 board is dictated by the VCO, but the overall maximum is 500 MHz. However, at frequencies close to 500 MHz the sidebands from the discrete nature of the signal become significant.

One of the original issues with the multiplication design was that instabilities in the low frequency source would be multiplied with the signal. As mentioned, the DDS is driven by a constant oscillator that it uses as its digital clock. The stability of the DDS output signal is related to the stability of that clock oscillator. Therefore, a special oven VCO was purchased for $\sim$ \$1000 from Vectron International. With this new oven oscillator, the DDS is stable to within ten parts per billion[18] over the year. Although the oven oscillator adds significant cost to the project, its signal can be shared among any number of DDS boards. The 1.3 GHz and 6.8 GHz sources will share the same stable signal.

Because the oven oscillator comes at a specific frequency of 61.44 MHz, it cannot be used to drive the DDS chip. A VCO at $\sim$ 1 GHz is divided down 16 times and

phase locked to the stable oven oscillator. The phase lock works by integrating the phase difference between the two signals and using that as an error signal to change the voltage input into the VCO. The VCO voltage input changes its output frequency within a small range. The phase lock loop is included as part of the AD9858 evaluation board.

Although the oven oscillator is very stable, it is not necessarily accurate. There is a voltage input into the oscillator which tunes the output frequency. For running the AD9858 it is not really important what the frequency of the oscillator is, but rather that the frequency is known accurately. This is because the commands that are sent to the AD9858 to set the output frequency are a function of the oscillator frequency. Since we assume the oscillator is 16×61.44 MHz, it is necessary for the oven oscillator to actually be 61.44 MHz. There is a good way to tune the signal using an AM radio[18]. First, we set the output of the DDS to a well known AM radio station frequency assuming that the oven oscillator is 61.44MHz. Next, we attach an antenna to the DDS output. Using a radio we tune to the radio station. An AM radio station works by adding sidebands to a fixed carrier frequency. To retrieve the sidebands, the radio station signal is mixed inside the radio. With the DDS signal nearby, it will also mix with the radio station and beat with the carrier of the AM station. The beat frequency is the spacing between the DDS output frequency and the radio station frequency. Using the tuning voltage on the oven oscillator, the frequency is shifted until the beat frequency goes away.

Details of the AD9858's operating characteristics may be found in table 3.1. When the board is ordered, it needs to be mounted inside of a box, with a power supply of 3.3 and 5V. To buffer different components of the system in an effort to prevent ground loops, optical isolators are attached to both the inputs and outputs of the dds. The board, once mounted with optical isolators is illustrated in figure 3.2.

Price	$350 (USD)
Frequency Resolution	32 bits
Output Power	-8 dBm
Output Impedance	50 Ω
Communication Protocol	Parallel and Serial
Stability	10 ppb/year
Maximum Frequency	~ 500 MHz

Table 3.1: AD9858 Design Features

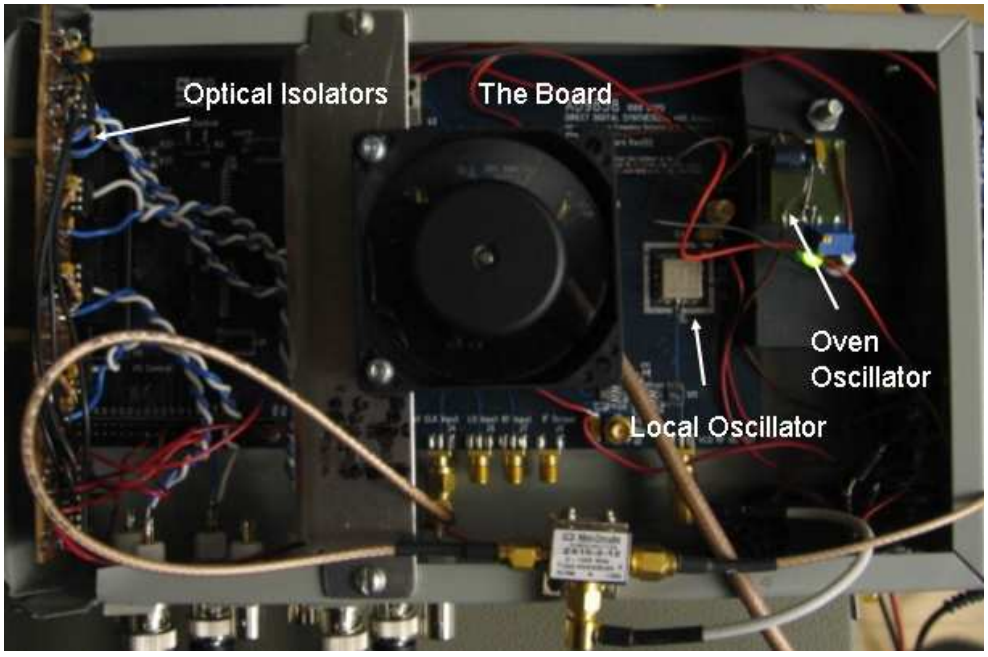

Figure 3.2: AD9858 Evaluation Board mounted in a metal box with power supply and optical isolators

Harmonics	The difference in power (dB) between the desired output harmonic and the undesired output harmonics.
Conversion Loss	The power loss associated with the device. Typically, these take a lot of power from the signal ($\sim$ 10dB)
Min/Max Power Input	Often frequency multipliers work within a very specific input power range. This is in order to most efficiently maximize the desired output and minimize harmonics.
Input Frequency Range	Frequency range in which the doubler operates.

Table 3.2: Frequency multiplier figures of merit

Multiplying RF and Microwave Signals

In their most basic form an electronic frequency multiplier is just a diode with a bandpass filter on the output. As the signal goes through the diode it undergoes a nonlinear change, which from fourier analysis creates signals at integer multiples of the original frequency. A bandpass filter on the output selects the desired signal. Often, these devices have a small input power window and a large conversion loss ($\sim$ 10-15 dB). Figures of merit for frequency multipliers are found in table 3.2.

Filters

One of the major issues with the concept of frequency multipliers is the generation of unwanted harmonics. Harmonics are also created by nonlinearities in amplifiers. In this application there is not a great concern for this issue because likely the harmonics are far enough off resonance that they do not effect the atom. However, if too many signals are created and propagate through the system, they can greatly affect the performance of subsequent components. The solution is to filter unwanted signals out of the system. Filters come in two varieties, low pass and high pass. A low pass filter removes high frequency noise from the signal and in the simplest case is just an inductor. A high pass filter does the opposite. In the simplest case a high pass filter is just a capacitor. The figures of merit for filters may be found in table 3.3.

Insertion Loss	Difference in power between the output and input (dB)
Stop Band	The range of frequencies for which there is greater than a certain amount of insertion loss (typically 20 or 40 dB).
Cut of Frequency	The frequency at which the insertion loss is 3dB (half the signal filtered out).
Pass Band	The range of frequencies for which there is less than 1dB insertion loss.

Table 3.3: figures of merit for filters

F_l-F_u	Lower bound and upper bound frequency range for the amplifier.
Gain	The power increase (in dB) of the input signal
1dB Compression Point	The output power (in dBm) when the gain has decreased by 1dB
Noise Factor	Ratio of signal to noise at the input to signal to noise at the output.
Directivity	How the impedence of the source affects the output impedance
VSWR	Voltage standing wave ratio, characterizes the reflections causes by the amplifier not being 50Ω matched.

Table 3.4: figures of merit for amplifiers

Amplifiers

In our design for a microwave source, amplifiers have a dual purpose. The first is that we need a certain power to evaporate atoms from the chip. As the signal goes through all the multiplication elements it loses a lot of power and amplifiers are needed to restore this power. The second purpose of the amplifiers is to get the signal at the right level to send into the multiplication elements. Some of these had a power window of 2 dB, so it was necessary to carefully amplify between each stage of the process. Figures of merit for amplifiers may be found in table 3.4.

3.2.4 Tools

When constructing and testing the high frequency sources a variety of tools were used.

Coupling	The ratio of the input power of the main line to the output power of the coupled port (dB)
Mainline Loss	Loss of signal along the main line
Directivity	Ratio of power (in dB) on the coupled port when the power is going in the desired direction to when the power is reversed.

Table 3.5: figures of merit for directional couplers

Directional Couplers

Directional couplers allow part of a signal from a line going in a certain direction to be sampled. Typically a coupler removes a small fraction of the signal, but a 3dB coupler splits the signal half and half. The essential design of a coupler is two striplines very close to each other so that some of the evanescent field leaks from one line to the other. Directional couplers are excellent for testing reflections. The figures of merit for directional couplers may be found in table 3.5.

Power Meter

A true power meter measures the amount of high frequency power is in a given signal. For frequencies less than 1.6 GHz, a product from Analog Devices (AD8362) was purchased. This product is not a true power meter, but it was a true V_{rms} meter. Therefore, for a single frequency into 50 Ω impedance it was proportional to the power. The input of this detector was an SMA connector and the output was a DC voltage. A calibration curve that plots output voltage versus input power may be found in Lab Book #1, page 175.

Spectrum Analyzer

When working with high frequency electronics, a spectrum analyzer is a necessary piece of equipment. It measures the power in each frequency component for a time varying signal. While this is not enough information to give the actual form of the signal versus time (there is no phase information), it is extremely useful. In this project the spectrum analyzer was used to measure the relative strengths of the

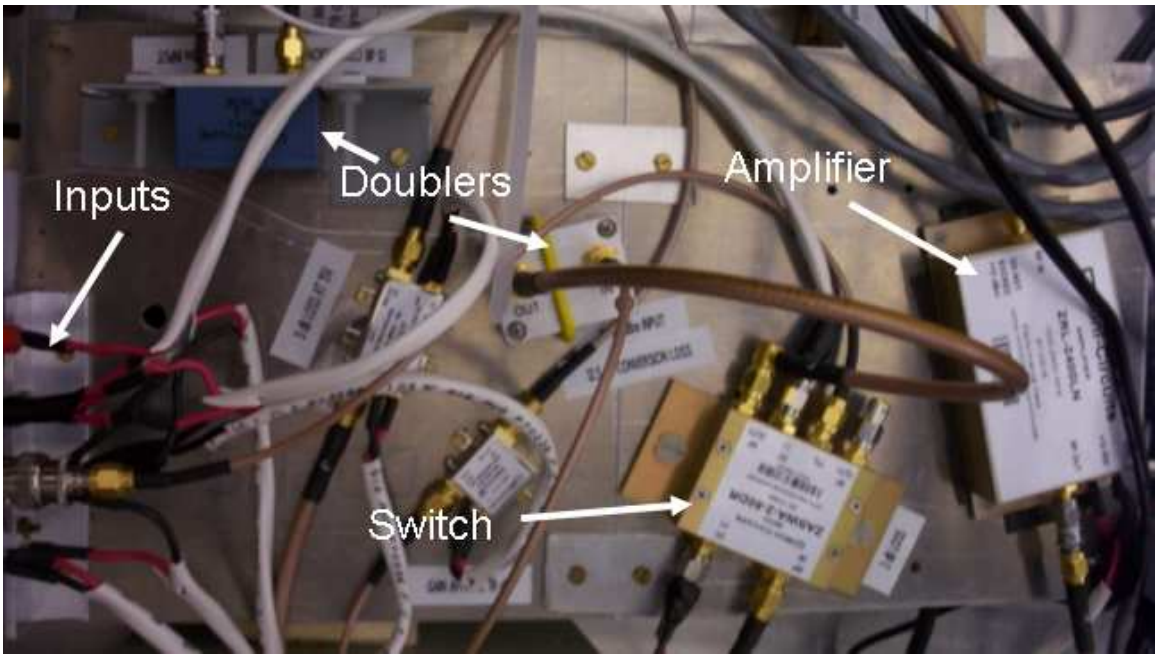

Figure 3.3: 1.3 GHz source constructed in summer 2005

spurious harmonics after each component in the system.

Commercial Synthesizer

To facilitate easier testing of the multiplication elements in the circuit we purchased the HP8656B, which is a 0-999 MHz signal generator. It did not replace the DDS board because it cannot switch fast enough for evaporation. However, during testing a steady input signal was needed.

3.3 1.3 GHz Source

The original design and construction of a 1.3 GHz source was part of the undergraduate thesis for Ian Leroux[17]. The AD9858 board was purchased and assembled and connected to the stable oven oscillator. All the parts for the frequency multiplier board were selected and purchased. They were assembled and purchased as part of the author's NSERC project in summer 2005. A photograph of the multiplication elements is illustrated in figure 3.3.

3.3.1 Coupling Into the System

One of the biggest issues with high frequency electronics is reflections. If you work out the transmission line equations, you see that unless the source is impedance matched to the transmission line and the source, then reflections will occur. The generally accepted impedance is 50 Ω and most coaxial cables are at this impedance. However, when is it that reflections become an imporant issue? Generally, reflections are not a big issue if the characteristic size of the system is much smaller than the wavelength of the oscillations. Some wavelengths corresponding to frequencies used in our labs are 30 MHz $\longrightarrow$ 100 m, 1.3 Ghz $\longrightarrow$ 30 cm and 6.8 GHz $\longrightarrow$ 5cm.

Evaporation in the experiment is done by putting the signal on a wire that goes through a DC electrical vacuum feedthrough and to the chip. Because the dimensions of the system are much smaller than 100 m, there were no large issues with coupling radio frequency signals into the system for evaporation between Zeeman levels. However, the impedance mismatch causes huge issues for the 1.3 GHz and 6.8 GHz signals, which have wavelengths on the order of the system size.

The reflection coefficient from a mismatched source of impedance Z is given as,

$$\Gamma = \frac{Z - 50}{Z + 50} \tag{3.1}$$

The reflection coefficient, Γ is in general a complex number. To measure Γ we can look at the reflection from the load. We did this using a directional coupler and using our V_{RMS} detector. We calculated that V_{RMS} as a function of z from the load is,

$$V_{RMS}(z) = \frac{A}{\sqrt{2}}\sqrt{1 + 2|\Gamma|\cos(\Theta_\Gamma + 2\beta z) + |\Gamma|^2} \tag{3.2}$$

The impedance of the load (at 1.3 GHz) was measured to be, $Z = 15.14 - 17.87i$. The idea of stub tuning is to add an open section of transmission line of a certain length a certain distance from the load to make the load matched to 50Ω impendance. One of the drawbacks of stub tuning is that it only works for limited frequency ranges.

Figure 3.4: Stub used to tune the 1.3 GHz system

For this system we were able to get a stub for tuning to 1.277 GHz. Figure 3.4 is an image of the stub that we used. Figure 3.5 shows the plot of power reflected versus frequency. A minimum of less than 5% reflection is clearly visible at 1.277 GHz. This demonstrates the viability of this method to couple microwaves into the system. Although this is still less desirable than getting fully matched vacuum feedthroughs.

3.3.2 Dual Evaporation

Once we had developed the 1.3 GHz source and stub tuned the vacuum system, we needed to see if they would have any effect on the atoms. Therefore, as a proof of concept, we measured the number of ^{40}K atoms in the trap after holding the 1.3 GHz source at a specific frequency. The results are shown in figure 3.6, which clearly shows that the field has some effect on the atoms. This is a positive preliminary result towards total manipulation of the hyperfine states.

3.4 6.8 GHz Source

The 1.3 GHz source was completed in the summer 2006 by the author as an extension of the thesis by Ian Leroux[17]. However, the 6.8 GHz source was designed, planned and constructed entirely as a component to this thesis. The following section will

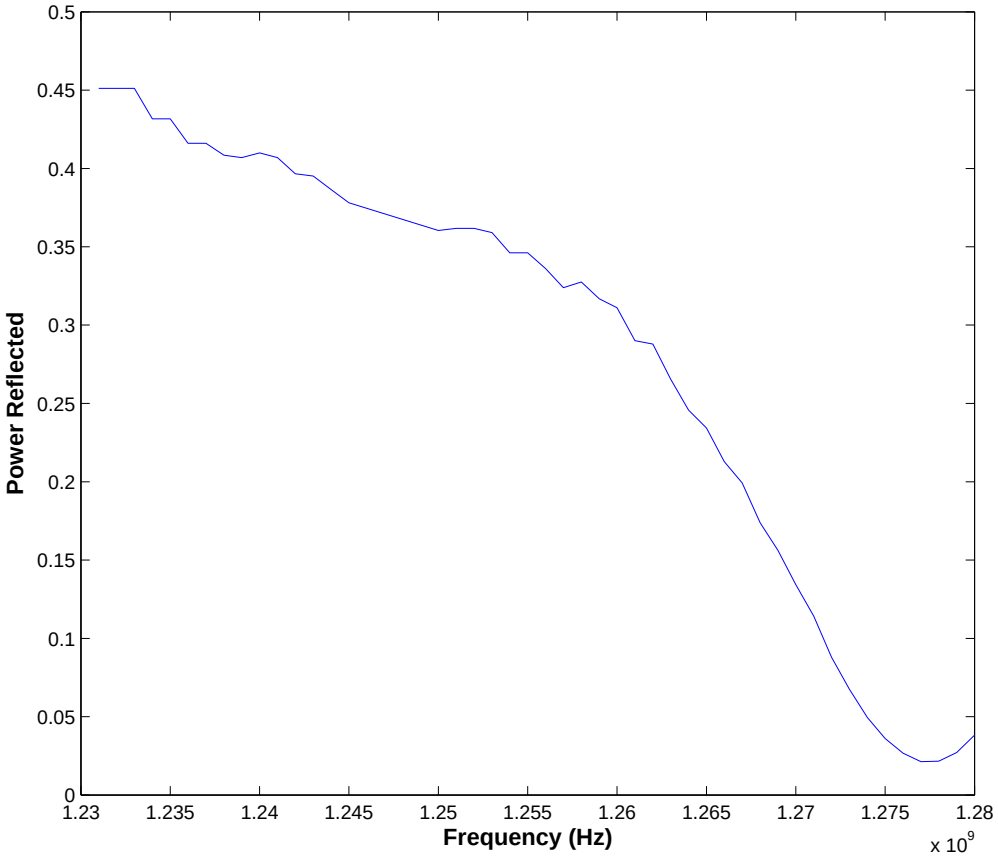

Figure 3.5: Reflection from the vacuum system versus frequency

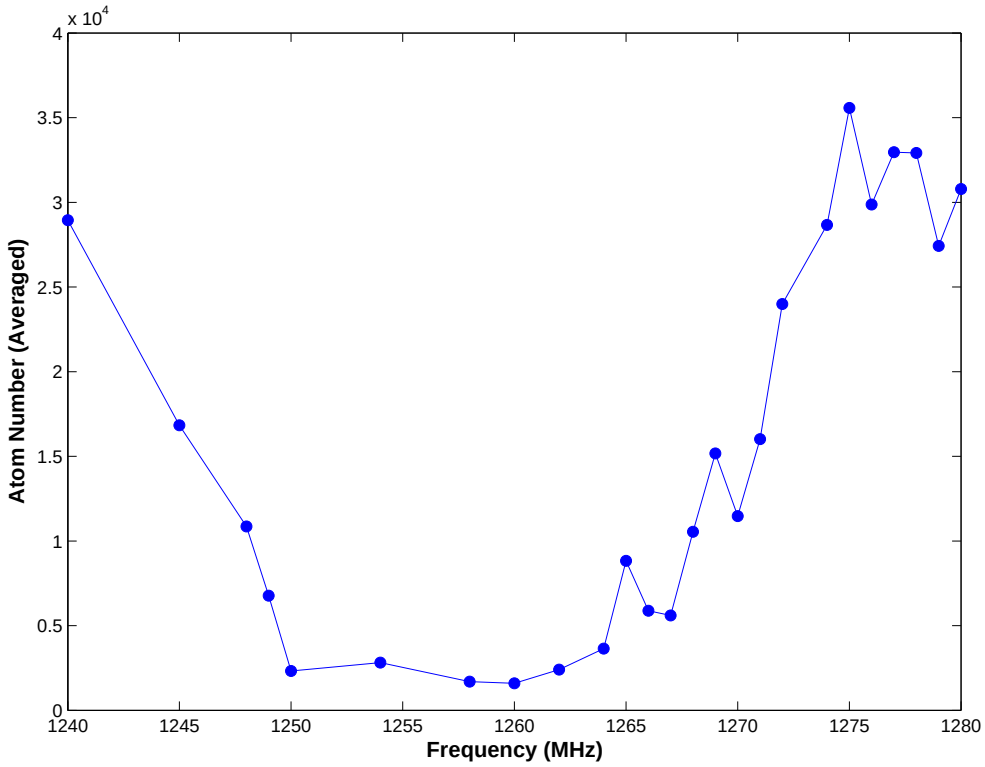

Figure 3.6: Ejection of ^{40}K from the trap using the 1.3 GHz source

outline the planning, construction and testing of this source.

3.4.1 Initial Design

After considering all the possible designs (see section 3.2.2), the frequency multiplication scheme was again selected. The base of the system would be another AD9858 DDS from Analog Devices, locked using the oven oscillator purchased for the 1.3 GHz source. Most of the components were selected from Mini-Circuits. However, this new source presented a problem because Mini-Circuits components tend to be limited to frequencies less than 2 GHz. Several microwave companies were consulted including Techtrol Cyclonetics, Marki Microwave, Pulsar Microwave and Miteq Microwave. Eventually, we selected the ATA1424 from Marki-Microwave, which was a pre-assembled amplifier-tripler-amplifier for input frequencies of 1.4 to 2.4 GHz corresponding to output frequencies of 4.2 to 7.2 GHz. This was well-suited for the requirements of the system since it covered just the frequency range that Mini-Circuits components would not. Since Mini-Circuits sells doublers only, the initial multiplication of the signal had to occur as a power of 2. Therefore, we decided on a total multiplication of 24, based on 8 times multiplication using 3 Mini-Circuits doublers and the final factor of 3 using the tripler from Marki-Microwave. The initial AD9858 frequency is therefore in the range of 280 MHz, which is well below the maximum value. This is better since near the maximum values, issues arise due to the discrete nature of the DDS output

One of the main issues when constructing a system based on signal multiplication is spurious harmonics that are created in the system. The system was initially designed and constructed with no filtering. This was based on two thoughts. The first thought was that filters can always be added after the fact. The second thought was that most of the frequency multipliers we used had much lower spurious harmonics. We figured that these would disappear through the amplification process. To an extent the first idea was correct. However, the second thought was absolutely wrong. Both of these issues will be addressed in section 3.4.2.

3.4.2 Construction

The first step to constructing the source was to select an appropriate means of mounting and connecting all of the various components. The idea was to place everything in a single box, with the inputs being the serial communication for the DDS and the power inputs and the output being the 6.8 GHz signal. A suitable container was found second hand, which was $\sim$ 30cm x 30 cm x 10 cm. The only required electronics for the source is power supplies for all the components and opto-isolators for the serial inputs into the AD9858.

Connecting Components

All the components used in the 6.8 GHz source are modular units requiring a high frequency input via an SMA connection and power and a high frequency output also via a SMA connector. There are several methods of connecting the components. The first method is to use flexible coaxial cable. Coaxial cable comes in many different formats with different properties. A summary of the figures of merit for coaxial cable may be found in table 3.6. For low frequency connections in the source we use RG-316 to connect some components. This coaxial cable is easy to use because of its flexibility. For the high frequency output we use RG-142, which is triple shielding to prevent high frequency leaks. Another variation on coaxial cable is semi-rigid cable, which has solid outside shielding. It may be molded into shape, but retains that shape after. Also, waveguides may be used for the highest frequencies, but we opted against this because waveguides are difficult to use. The final is to connect components directly using SMA adapters. This is a good method if the components are going to be close together. Since the components in the source are close together, we opted to connect many of them in this way.

Attenuation	Given in dB per m, this is the power loss as the signal propagates through the cable (frequency dependent)
Maximum Frequency	Typically, this frequency is when non-TEM modes are able to propagate in the line
Impedence	The impendance per unit length of the cable, always 50 Ω for our applications
Center Conductor	The material of the center conductor and whether it is solid or stranded
Dielectric	The material of the dielectric between the center and outer conductor
Shielding	Giving in dB per m, this is the ratio of power in the cable to the power that leaks out of the cable

Table 3.6: figures of merit for coaxial cable

Electronics

Three electrical components were constructed for this project. The first is the circuit for the AD9858, which regulates the voltage into the AD9858 and provides optical isolation for its inputs. This circuit connects to a 9V DC regulator that plugs into the mains and has regulated outputs of 5V and 3.3V. The circuit also provides power for a fan that cools the AD9858 chip, an LED that indicates power on/off and has a connection to a switch that turns the power to the DDS on and off.

Next, the various multipliers, amplifiers and switches for the system had voltage and current requirements listed in table 3.7. To satisfy these power requirements a AC-DC power supply was purchased from Digi-Key (part #179-2069-ND) with outputs of 24 and -24 volts and 1.2A each. Additional regulators at 5V, 15V and -5V were added to provide the required voltages. Finally, there is a variable attenuator in the design that requires at 0-17V signal, which linearly determines the attenuation (in dB). Because the input impedence of this signal is fairly low it is not as simple as using a potentiometer. Instead a unitary gain op-amp circuit was constructed to connect to the potentiometer.

Voltage (V)	Current (mA)
-5	60
5	515
15	150
0-17	30

Table 3.7: Voltage and current requirements for the components of the 6.8 GHz source

Mounting Components

One of the difficulties in construction was to fit all the components into one box. This was accomplished in two ways. First, the AD9858 board was placed above the circuit with its power supply and opto-isolators. Second, all the other components were connected directly using SMA adapters. One issue with this is that each component lies at a different level. To prevent stress of the connections, small plastic mounts were made for each component so that the connections all occur at the same level.

3.4.3 Final Product

After all the parts of the system were assembled the source was tested using the spectrum analyzer. As mentioned in section 3.4.1, the initial design did not call for any filters, except for on the AD9858 output and on the final output. The thought was that spurious harmonics would be suppressed by the amplification stages. Initial spectra of the output indicated that this was not the case. The final output contained nearly every single harmonic, spaced equally at the original frequency of 283 MHz (6.8 GHz $\div$ 24). What was the most surprising is that all of these harmonics had nearly equal power. Because the input to each component of the system was a multi-frequency signal, the component behaviour was not as predicted. In fact, we speculate that the amplifiers were giving more gain to the lower power frequency components than the higher value frequency components leading to an equalization of all the frequencies. We decided that bandpass filters were required at each multiplication stage resulting in bandpass filters of 567, 1133, 2266 and 6800 MHz. These filters were constructed from high pass and low pass filters available from Mini-Circuits.

A summary of the components used in the construction of this source is found in table 3.8. Figure 3.7 shows a photograph of the completed system and figure 3.8 illustrates a schematic of the connected components. Spectra from the final system may be found in appendix A. The final output spectra is shown in figures A.8 and A.9. Spectra at locations A1,A2,B1,B2,C1 and C2 from the schematic (figure 3.8) are shown in figures A.2,A.3,A.4,A.5 A.6 and A.7 respectively. The system was finished in November 2005, however, it cannot be used to manipulate atoms because there is no method to couple the microwaves into the system due to reflections. Therefore, a new system needed to be constructed that is microwave compatible. These issues were addressed by the project detailed in the next section.

3.5 Conclusions

In this section, we have presented the design and construction of both a 1.3 GHz and 6.8 GHz source for the eventual manipulation of the hyperfine levels of ^{40}K and ^{87}Rb respectively. Both of the sources have been demonstrated to be operational and the 1.3 GHz source has even shown a basic ability to manipulate atoms in the trap. However, the ultimate goal is still the full control of hyperfine transitions for ^{40}K and ^{87}Rb . Part of this goal depends on the construction of a new stack, which will be addressed in the next section. However, once this has been completed we need to use these sources to measure the Rabi frequency of these sources. Then, we may consider whether further amplification of the signal is needed.

Part #	Company	Description	Cost (USD)
AD9858	Analog Devices	Direct digital synthesizer	$49.95
VLF-320	Mini-Circuits	Low pass filter	$21.95
ZFL-500HLN	Mini-Circuits	Low noise amplifier	$99.95
MK-2	Mini-Circuits	Frequency doubler	$52.95
ZX60-2522M	Mini-Circuits	Amplifier	$59.95
SHP-500	Mini-Circuits	High pass filter	$38.95
VLF-490	Mini-Circuits	Low pass filter	$21.95
MK-5	Mini-Circuits	Frequency doubler	$76.95
ZX73-2500	Mini-Circuits	Variable attenuator	$49.95
ZX60-2522M	Mini-Circuits	Amplifier	$49.95
VLF-1000	Mini-Circuits	Low pass filter	$21.95
VHF-880	Mini-Circuits	High pass filter	$24.95
FK-3000	Mini-Circuits	Frequency doubler	$79.95
ZX60-2510M	Mini-Circuits	Amplifier	$59.95
VHF-1760	Mini-Circuits	High pass filter	$24.95
VLF-2250	Mini-Circuits	Low pass filter	$21.95
ZASWA-2-50DR	Mini-Circuits	High frequency switch	$89.95
ATA1424F	Marki Microwave	Amplifier, tripler, amplifier	$324.00
VHF-5500	Mini-Circuits	High pass filter	$24.95
VLF-6700	Mini-Circuits	Low pass filter	$21.95

Table 3.8: Summary of components used in the 6.8 GHz system

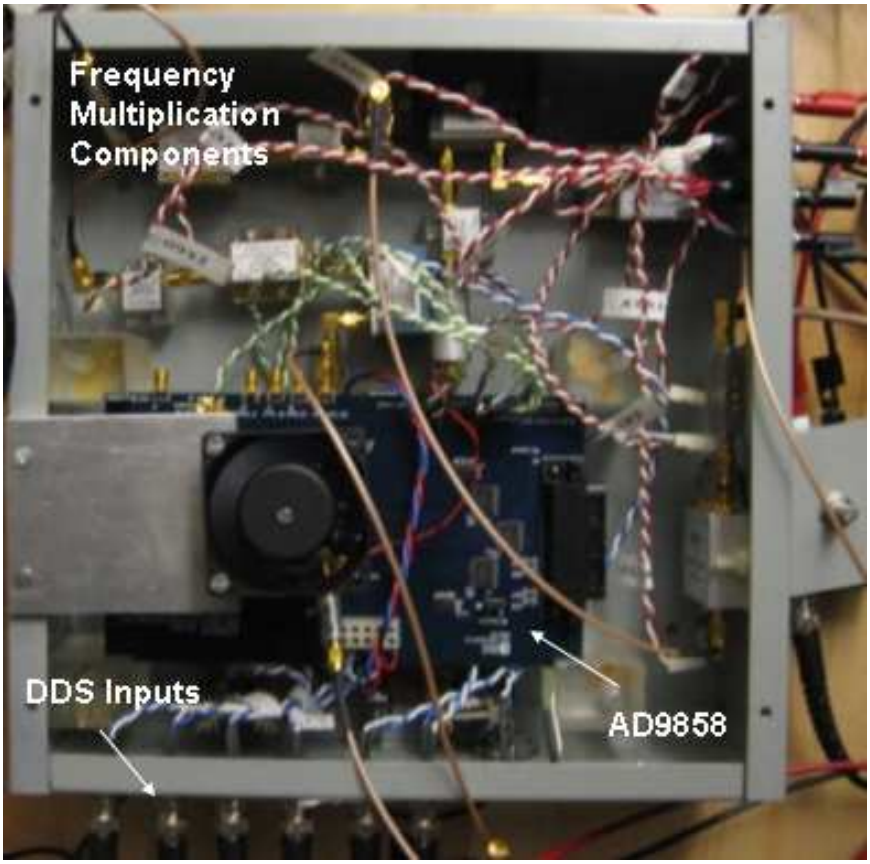

Figure 3.7: Photograph of the complete 6.8 GHz system

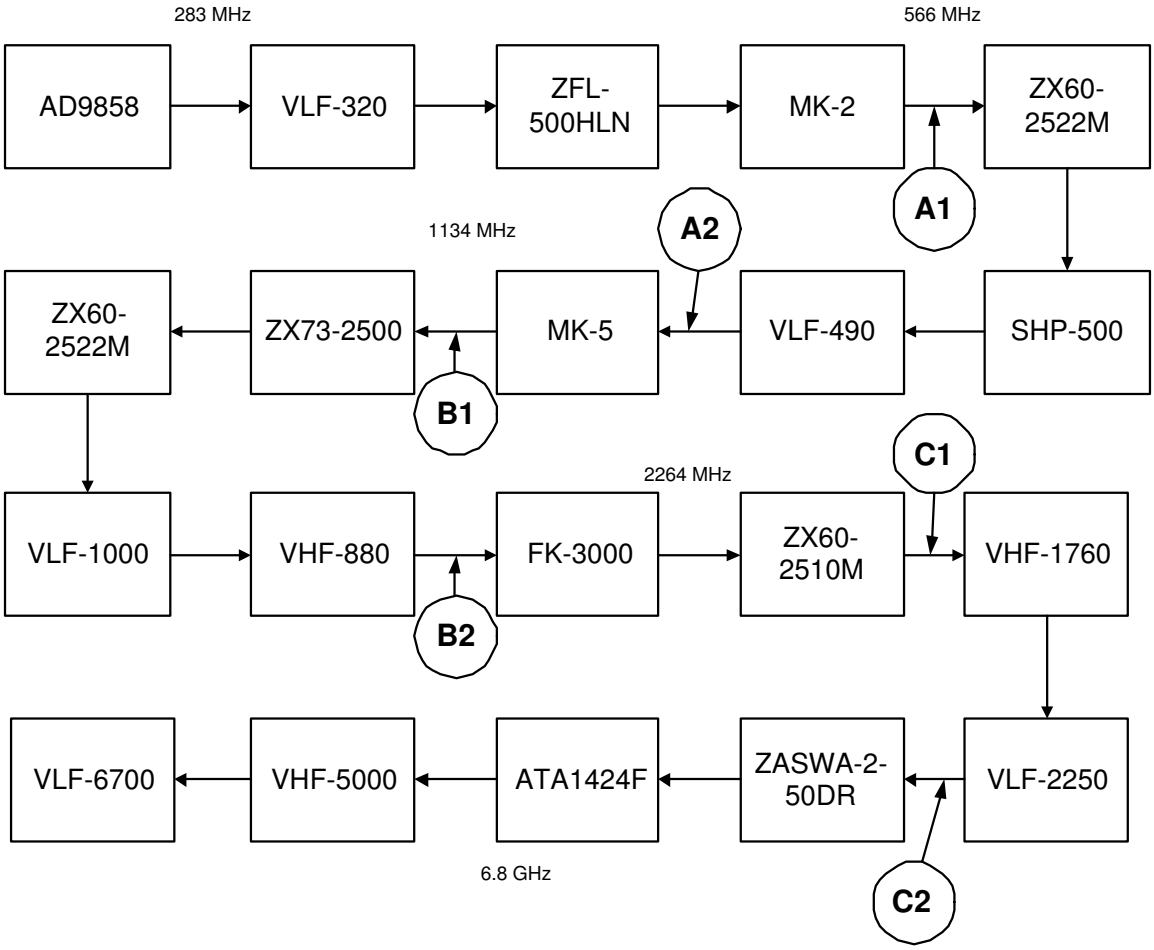

Figure 3.8: Schematic of the complete 6.8 GHz system

Chapter 4

New Stack Apparatus

One method of generating the magnetic fields required to trap neutral atoms is to use current running through wires fabricated to a substrate. The benefit of this technique is that the wires may be made very small, which increases the gradient of the trapping field. Also, many different trap configurations may be consolidated onto one substrate. Cold atoms experiments that use these microfabricated wire traps are known as 'chip' trap experiments. In addition to their benefits, chip traps also bring complexities to the experiment. One of these complexities is the requirement that the chip be supported inside the vacuum system. There is at least one group that accomplishes this task by making the chip one wall of the vacuum system [19]. However, the majority of chip traps support the chip inside the middle of the vacuum system by mounting the chip to some sort of structure. These structures are commonly referred to as chip stacks. Besides mounting the chip inside the vacuum system, chip stacks also function as heat sinks for the chip wires, guide electrical signals to the chip and hold the atomic dispensers. The entire apparatus includes not only the chip and the stack, but also the vacuum flange that the stack mounts onto and the electrical feedthroughs that carry the chip signals through the air to vacuum interface.

The initial chip stack for the Thywissen group was constructed by graduate student Marcius Extavour[20]. This stack was mounted to a 6"-$2\frac{3}{4}$"reducer flange with a 20-pin electrical feedthrough on the $2\frac{3}{4}$"port. The stack was constructed from OFHC

(oxygen free high conductivity) copper and macor, which is a machinable ceramic. The macor was used to clamp the chip to the stack without making electrical contact. The wires used were ceramic coated nickel-copper. While this stack has performed very well, there were reasons why it needed to be replaced. First, the chip design has changed. The original chip, which was supplied by the Alain Aspect group from the Institute D'Optique in Orsay, France, had 8 electrical connections on the top of the chip, 4 on each of the short sides. The new chips, manufactured at the University of Toronto, have 24 connections, all on the bottom of the chip to improve optical access to the top where the atoms are trapped. A schematic of the new chip is illustrated in figure B.1. The second reason to replace the stack is because the old system was not compatible for use with microwave signals. The 20-pin electrical feedthrough was not designed for use with high frequencies, which just reflect from the air-vacuum interface. The following details the design and construction of a new stack for use in the Thywissen lab.

4.1 Design

The design of the new stack began in summer 2005. As mentioned in the previous section, the design was motivated by a new chip design and requirements for high frequency signals at the chip. The first step to the design process was to identify the requirements of the stack. Some of these requirements were the same as before, such as being UHV (ultra high vacuum) compatible and some of these requirements had changed, such as the new chip requirements. Once requirements had been identified, a new flange to support the stack was selected. Then, a design was selected and plans were developed in a CAD program.

4.1.1 Requirements

The first stage of designing the new stack was to list the required elements for the stack. These include:

- UHV compatible
- Low vibrations
- Couple microwaves to the chip
- Hold and heat sink the chip
- Guide current to the chip contacts to create the magnetic trap
- Hold the dispensers and guide current to them
- Conform to the dimensions of the system

4.1.2 A New Flange

One of the main issues with the microwave compatibility is at the air-vacuum interface. To prevent power reflections in a high frequency system, the transmission lines need to be everywhere 50 Ω. However, the 20-pin feedthrough is not impedence matched and is therefore terrible for high frequency electronics. The first stage of the design was to find a suitable feedthrough for high frequency signals. Insulator Seal sells two types of high frequency feedthroughs with SMA on both sides. The first uses Alumina as the insulator and is therefore not exactly 50 Ω matched, but it is UHV compatible. The other feedthrough uses Teflon as an insulator, which allows it to be 50 Ω, but the vacuum properties of Teflon are debatable. After some discussion and consulting some literature[21][22], we decided to use two alumina feedthroughs, for RF and 1.3 GHz signals and the Teflon feedthrough for the 6.8 GHz signal. These feedthroughs are each on a $1\frac{1}{3}$"CF flange. In addition to these new feedthroughs, the new stack still needs all the old lines to the chip to control the chip wire currents. Therefore, another 20-pin connector was selected from Kurt Lesker (part IFTAG204103), which uses a $2\frac{3}{4}$"CF flange. The vacuum system for the experiment consists of a 6" cube, so all these components have to be attached to a 6" CF port. A multiport flange from MDC was selected. This is a 6" flange with a $2\frac{3}{4}$"port in the center and 6 $1\frac{1}{3}$"ports coming out at angles. Since we only need 3 of

Figure 4.1: Flanges for new stack system[3]

the 6 $1\frac{1}{3}$"ports, we decided to purchase 2 $1\frac{1}{3}$"4 conductor 15 A feedthroughs for the dispensers. Currently the dispensers are being run through the 20-pin feedthrough, which is only rated up to 10 A per pin. When the dispensers are almost empty, up to 15 A are used to get as much out as possible. Photographs of these flanges may be found in figure 4.1. A schematic of the multiport flange in CAD is illustrated in figure B.2.

4.1.3 System Dimensions

The next step when designing the new stack was to identify the relevant dimensions of the vacuum system. Figure 4.2 illustrates the vacuum system with dimensions including current distances from the bottom of the cell to the chip face. It is important to keep the new dimensions as close as possible to the old dimensions so that the current alignment of optics and fields does not need to change appreciably.

4.1.4 Summary of Groups with Stacks

Before building something new, it is always good to review previous designs to see what works. To this end, the author looked at other groups who have implemented stack like designs into their cold atom experiments. This summary is provided in table 4.1. Some of the important things learned by investigating stacks used by other groups is that first, you can use more than just copper and macor and have a good

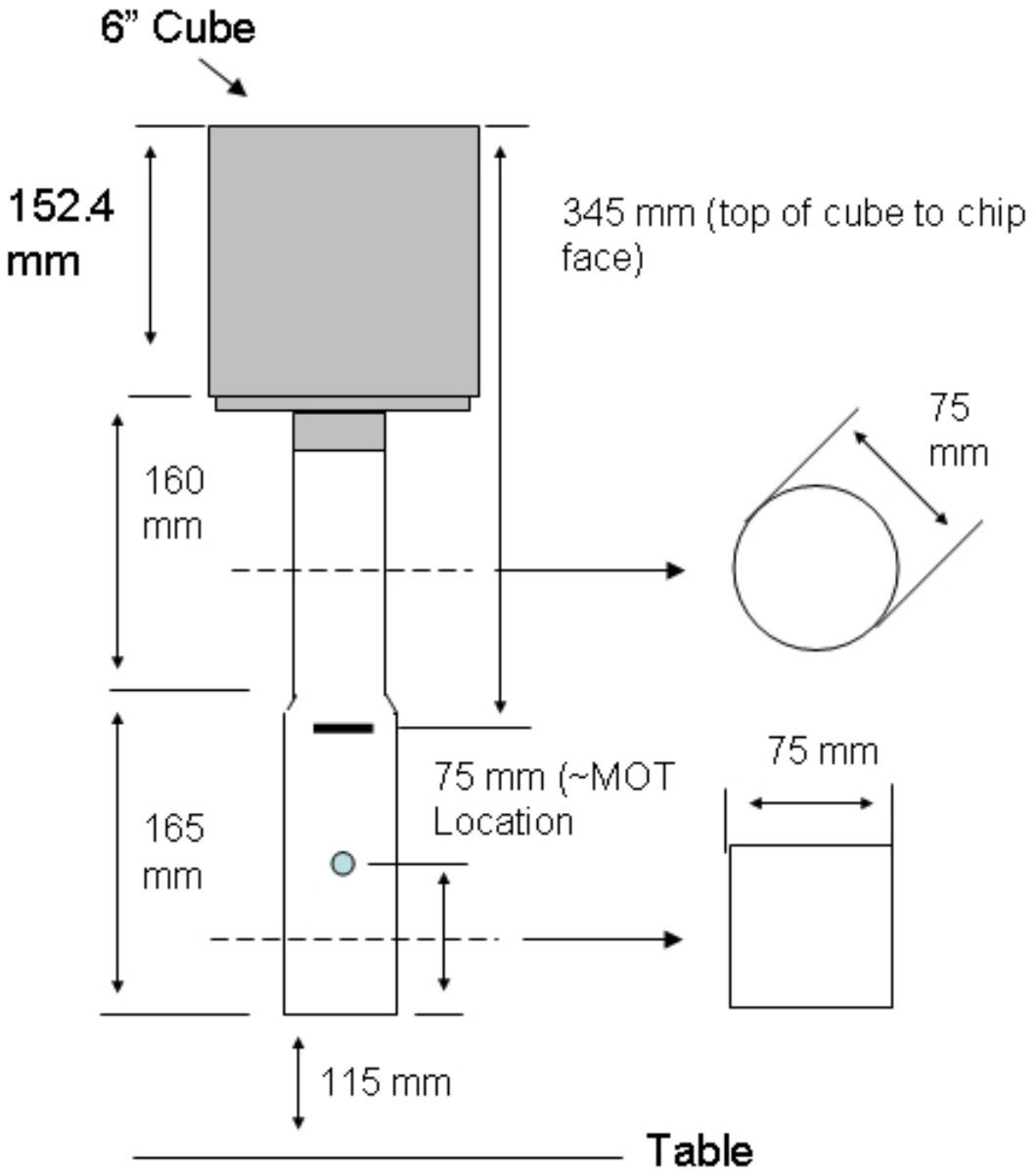

Figure 4.2: System Dimensions

Group	Website	Comments
Zimmerman	www.pit.physik.uni-tuebingen.de/ zimmerman/ forschung/index.html	MOT coils inside vacuum
Halina Rubinsztein-Dunlop	www.physics.uq. edu.au/atomoptics	Wires screwed to chip, ceramic coated wires, macor dispenser holders
Ben Gurion University	www.bgu.ac.il/atomchip/ index.html	Just starting out
Ted Hansch	www.mpq.mpg.de/Ehansch/ index.html	Guides wires along length of stack to chip
Orsay	atomoptic.iota.u-psud.fr/enmain.htm	
Stamper-Kurn	www.physics.berkeley.edu/ research/ultracold	Use anodized aluminum, but maintain good vacuum
Dana Anderson	dza.colorado.edu	Kapton wires soldered to chip, chip glued to copper stack
Jorg Schmiedmeyer	pi1.physi.uni-heidelberg.de/physi/ atph.index.php	Guide the wires using macor, chip sits on a macor block, wires connected using wire bonding
Ketterle	cua.mit.edu/ketterle_ group/home.htm	Wire connections with wire bonding (many broke when baked), chip screwed into an aluminum block, kapton insulated wires

Table 4.1: List of groups that have chip stacks

vacuum. Groups used everything from glue, solder, anodized aluminum and kapton, so we can assume these are likely all good for UHV vacuum. Next, the stack is more organized if the wires are guided all the way to the chip face. Also, the dispenser holders of the Halina Rubinsztein-Dunlop group are very elegant. This would be good to implement in our new stack because keeping the dispensers in place was an issue when trying to fit the current stack into the vacuum system. We should probably avoid the use of wire bonding based on the Ketterle experience of having them break during the vacuum baking process.

4.1.5 Final Design

With all the information about the new flanges, the system dimensions and stacks built by other groups it was time to determine the design of our new stack. The design was completed in a CAD program and all of the plans may be found in appendix B. The following will discuss the various aspects of the design more specifically. Each of the drawings calls for vent holes to be drilled into certain screw holes. This is a technique used for parts that will go into vacuum to prevent gas from being trapped and slowly leaking out into the vacuum system. This is known as a virtual leak and can prevent the system from achieving ultra high vacuum pressures.

Flange Connections

The first piece of the stack is the connection to the flange. The geometry of this piece is constrained by the flange since the ports must be free for wires. At the same time this is the base of the stack and must be sturdy to give structural stability to the rest of the stack. The spaces between the holes for the $1\frac{1}{3}$"ports presented a perfect spot on the flange to mount the stack. Because the space is not very big, only thin pieces could connect. To maximize the stability, a 'leg' for the stack was placed at each space. The stack itself must be close to the center of the flange to fit into the glass cell. However, the connections to the flange have to made at the edge of the flange. Therefore, the legs have to have an 'L' shape. The CAD drawing of the stack leg is found in figure B.3. The design calls for six of these made out of OFHC copper. The legs are tall to allow wire connections to be made in the center to the 20-pin feedthrough.

Stack Body

The main body of the stack needs to serve three purposes. First, it needs to hold the chip far into the vacuum system. However, it must do so with stability and as a heat sink. The chip connects to the stack by screwing into the body through the holes in the chip. Therefore, a solid block of copper with screw holes in the top is perfect,

except for the wire connections that have to be made on the back of the chip. To accommodate these connections, yet still have somewhere for the chip to screw into, just the area where the connectors are is milled away. This design is illustrated in figure B.5. Next, the body has to be connected to the legs. This is achieved through a reducer piece which screws into both the stack body and the set of six legs attached to the flange. The wires underneath the reducer need to come up to guide along the stack body so there are holes in the piece for wires to come through. This design is shown in figure B.4.

Wire Guiding

One of nice features of several stacks from other groups is the wire guides along the body of the stack. Therefore, wire guides were designed for this stack out of aluminum. At first it was thought that we were going to use bare copper wires. If this were the case, the wire guides would need to be insulated. This would be facilitated by anodizing these aluminum pieces. The bottom wire guide is shown in figure B.6 and the middle wire guide is shown in figure B.7. Both wire guides attach to the stack body with 0-80 screws. The middle wire guide is merely a set of holes to keep the wires close to the stack. However, the bottom wire guide also has holes for screws to go into each wire guide to either keep the wire in place or make a connection between two wires. At first it was thought that we would use bare copper wires from the bottom wire guide to the chip and insulated wires from the feedthroughs to the bottom wire guide. The connection would be made at the wire guide with pressure from the small screws.

Chip Connections

One of the most difficult design aspects of the new stack was the chip connections. The question is once the wires are guided to the chip, how do the wires maintain good contact with the electrical contact pads on the back of the chip. Several ideas were discussed, including soldering the wires, making wire bonds and using springs. At first we tried to avoid using solder in order to prevent introducing contaminants into

the system. Wire bonds have been known to break during bake out and the springs idea was too complex. Instead, a piece of foil would be put into contact with the pad via pressure from a single screw. The other end of the foil would then be connected to a wire coming up the stack body in a wire guide at the top. Like in the bottom wire guide, the top wire guide would have screws to press the foil and wire together. These guides are shown in figures B.8, B.9 and B.10. The top wire guide (figure B.8) is also designed to hold four dispensers. These pieces are designed to be anodized and thus be insulating. The issue with the top wire guide (figures B.9 and B.10) is that there is nowhere for it to attach to the stack body. Little washers were designed to go between the screw attaching the chip to the stack and the chip, which serve a dual purpose. First, they distribute the screw stress more evenly across the screw to increased heat sinking. Also, the top wire guides hang from these washers (figure B.11).

4.2 Construction

OFHC copper was purchased from the Southern Copper company. The materials and plans were then sent to the University of Toronto, Department of Chemistry machine shop where they were machined by machinist David Heath. The screws holes in the multi-port flange were done by the Department of Physics machine shop.

4.2.1 Anodizing Aluminum

As mentioned in section 4.1, insulated parts for the system were to be made from anodized aluminum versus macor. Anodized aluminum is a process whereby a layer of aluminum oxide is created on the surface of the Aluminum. The layer is formed by running current through the aluminum piece in a sulfuric acid solution. After an initial layer of about 1μm is formed the layer of aluminum oxide grows a porous layer, which can become quite thick. Therefore, aluminum pieces which have been anodized can be extremely resilient to wear. Standard anodization is done at room temperature with 180-200 g/L of H_2SO_4, 4-12 g/L of aluminum and 15 A/ft^2 of current

density. Approximately 39 minutes of this will grow at 18μm layer of aluminum oxide. Hardcoating is anodization done at approximately freezing. This results in a very hard layer of aluminum oxide and is generally only done in industry[23].

Anodizing Steps

The following is the steps that we followed when attempting to anodize some test pieces of aluminum.

1. Prepare 15% by mass solution of H_2SO_4.
2. Cut a 3L plastic bottle in half and lay two aluminum U-channels across. Do not use stainless steel anywhere because it will get eaten away.
3. Get a test piece of aluminum to be the cathode and the piece to be anodized as the anode. Hang both in the solution using aluminum wire. Make sure the aluminum wire is really pressed into the piece somewhere so that the wire does not anodize and lose electrical contact.
4. For about a 5cm x 3 cm x 0.5 cm piece it required 2A at $\sim$ 15 V for about 20 minutes.

Anodizing Results and Discussion

We never actually got to the point where we anodized the pieces for the stack. However, we did want to test that screw holes would be insulated. What we found was that sometimes the tapped holes would be insulting. However, if the anodization layer became too thick, the screw would dig into it and break it, causing electrical contact. We found that by re-anodizing these pieces once electrical contact was made just briefly seems to fix the problem. Although, more investigation is likely needed to make a conclusive finding.

4.3 Final Product

In the following are some pictures of the completed and assembled stack without the wires. The aluminum pieces still need to be anodized and the entire assembly of the wires, chips, stack and vacuum components needs to take place. Figure 4.3 shows the stack mounted to the multiport flange. Figure 4.4 illustrates how the stack attaches to the flange. Finally, figure 4.4 shows the top of the stack. When the stack goes into the system a chip will be sitting on the top and the wires will be guided through the aluminum pieces.

4.4 Conclusions

The stack has been designed, all the pieces machined and all the required components have been acquired from the various vendors. However, there is still a lot of work to be done. First of all, the stack has not been fully assembled. The current state of the assembly is that all the flanges have been cleaned and sealed together and they are waiting for the stack to be attached. This entails anodizing and testing the required aluminum pieces, building the SMA vacuum connectors and making all the wire connections from the flanges to the chip. It has been recently decided that the wires will be soldered, with special vacuum solder, to the chip. Once the stack has been fully assembled we need to test the high frequency feedthroughs and measure their actual impedence at the relevant frequencies. Also, we need to test the heat flow capabilities of the stack. Recent testing of the chip has revealed that the maximum chip current is strongly dependent on how well the stack behaves as a heat sink. Finally, we need to test the vacuum compatibility of the new stack materials. This will be addressed in the next section.

Figure 4.3: The stack (without wires) attached to the vacuum flange

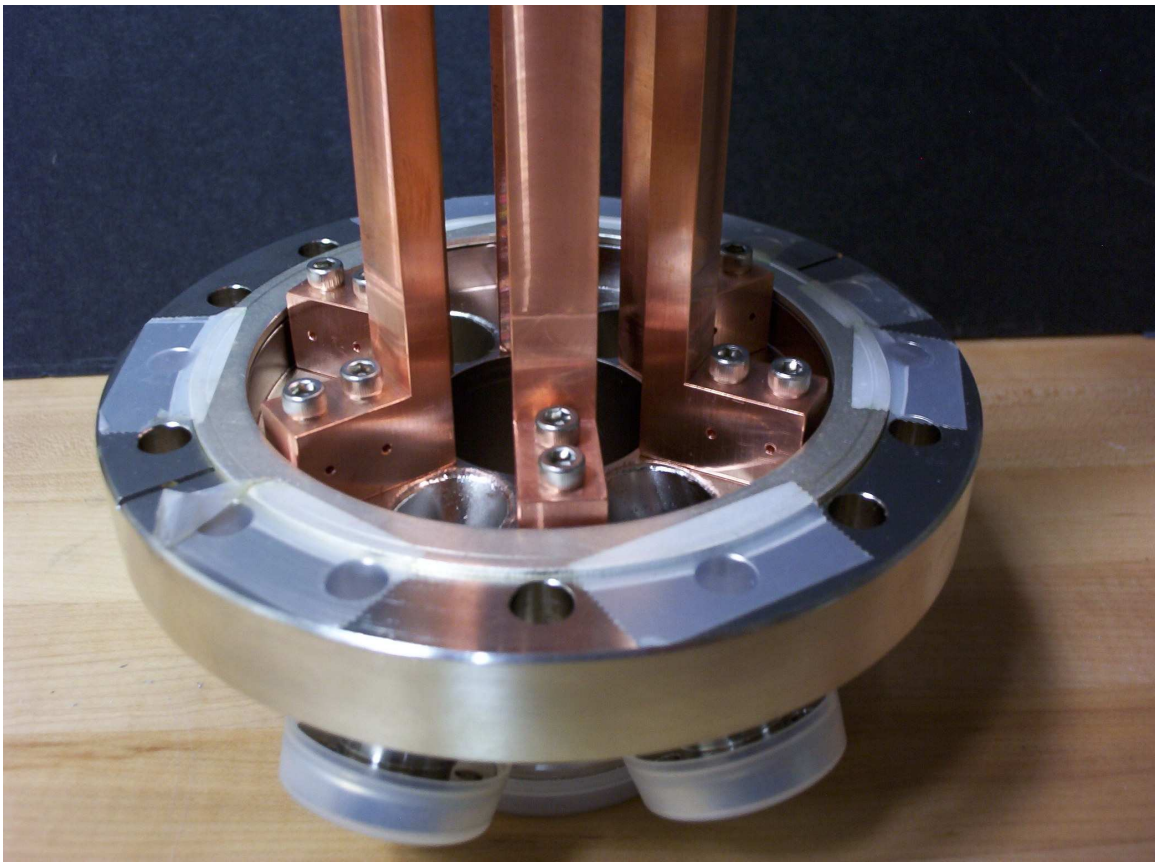

Figure 4.4: Closeup of how the stack attaches to the vacuum flange

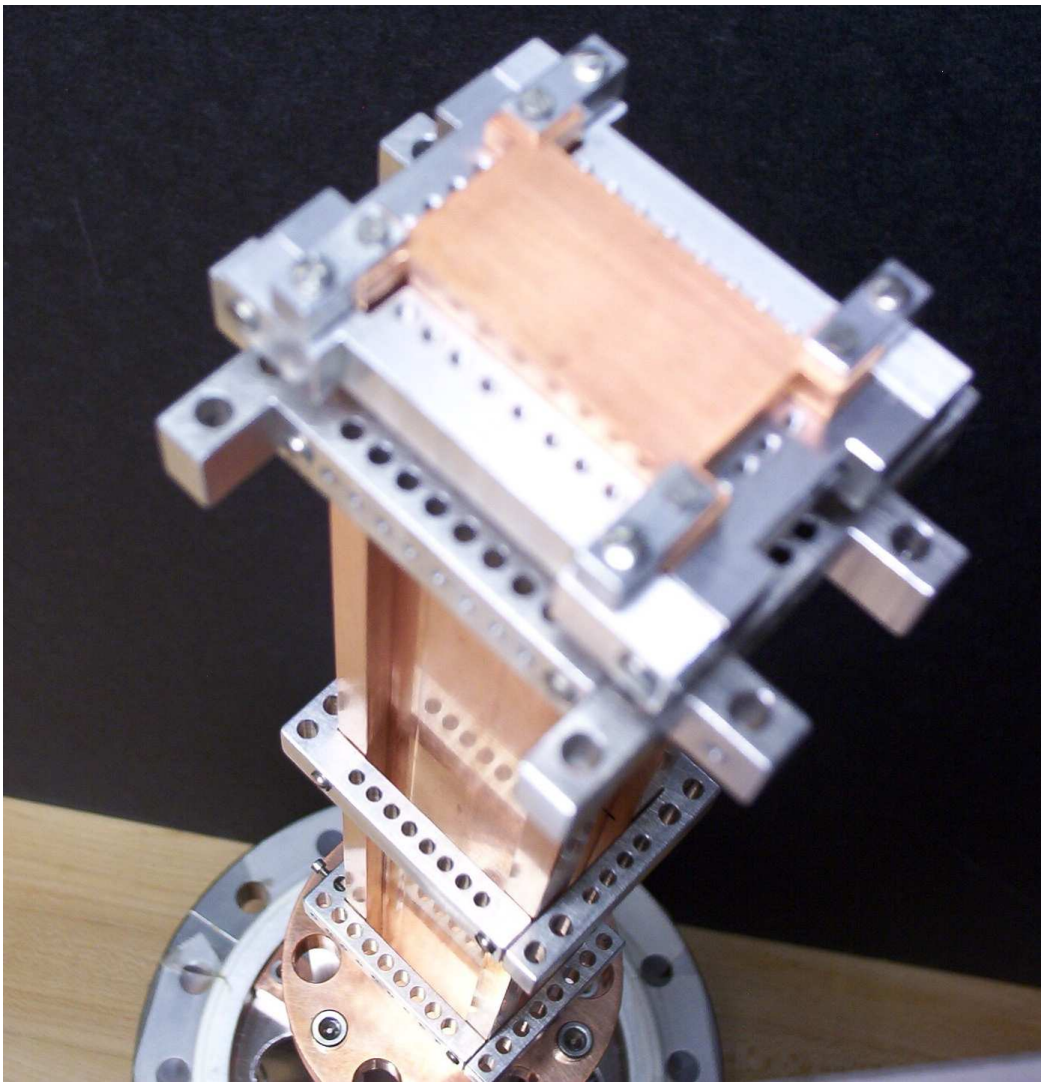

Figure 4.5: Stack from the top without a chip

Chapter 5

Vacuum Testing

Many new materials, such as teflon and anodized aluminum were used to construct the new stack. There are questions regarding the compatibility of these materials with ultra-high vacuum. Unfortunately, these are not answered questions. The material that is most contentious is anodized aluminum. Because of its porous nature it has a high surface area and is therefore a candidate for large outgassing. However, there are some groups, such as the Stamper-Kurn group at the University of California Berkeley who have used both anodized aluminum and Teflon with great success[24]. Ultimately, the best way to test these materials is to put them into ultra-high vacuum and measure the pressure. Because of the importance in maintaining a good vacuum for doing cold atom experiments, it is too risky to put untested materials into the main experiment. Therefore, a secondary vacuum system was constructed for the purpose of vacuum testing these materials. The 'pressure gauge' for this new system is the lifetime of a magneto-optical trap, which from section 2.3, we know is proportional to the pressure of the system. The plan was to first create a vacuum system without the stack to get a reference MOT measurement. Then, the system would be opened and the fully assembled stack placed inside. A second measurement of the MOT would be made and then compared to the first MOT to see if one of the stack materials significantly altered the system pressure. At the time of writing this document, the first MOT measurement has been made. The following details the construction of this new vacuum system, the setup of the magneto-optical trap and initial measurements

of the system pressure.

5.1 Building a New Vacuum System

The first step towards constructing the MOT pressure gauge was to construct a new vacuum system. Because we wanted this test to simulate the conditions of the main experiment, the new vacuum system was built to resemble the vacuum system of the main experiment. The central piece is a 6" cube from MDC Vacuum (part #409005). The top of the cube is a window (when the stack is not in the system) and will be the port for the multiport flange when the stack goes into the system. The glass cell is mounted to the bottom of the cube. This is an old glass cell that was used in the first setup of the main experiment in the Thywissen lab. It was replaced with a cell with better optical access.

One of the side ports of the cube is fitted with a residual gas analyzer from Stanford Research Systems (SRS). A residual gas analyzer is an ionizing gauge with a mass spectrometer. Therefore, it can read off the partial pressure of elements in the system of a given atomic mass. Another side port is fitted with a 6" $\rightarrow 2\frac{3}{4}$"reducer flange with a 4 pin electrical feedthrough. This will be used to provide current to a Rb dispenser inside the system. The pumps for the system are attached on the other two side ports opposite to each other. One side is a right angle elbow attached to an ion pump. The other side is a 6" $\rightarrow$ 41/2" conical reducer attached to a VAT viton valve which is attached to a turbo pump. The elbow and conical reducer provide the supports for the entire system.

As mentioned in the previous paragraph the pumps for the system are a turbomolecular pump and ion pump. The turbomolecular pump is backed by a mechanical roughing pump. When turning the system on, the roughing pump is turned on first. After approximately 10 minutes the turbo pump is started followed by the ion pump (more about this in section 5.1.4). The turbo pump is isolated from the system in the end by the valve since the limit of the turbo pump is $\sim 10^{-8}$ Torr. The ion pump is a Duniway 60 l/s galaxy diode. The galaxy refers to the pattern etched into

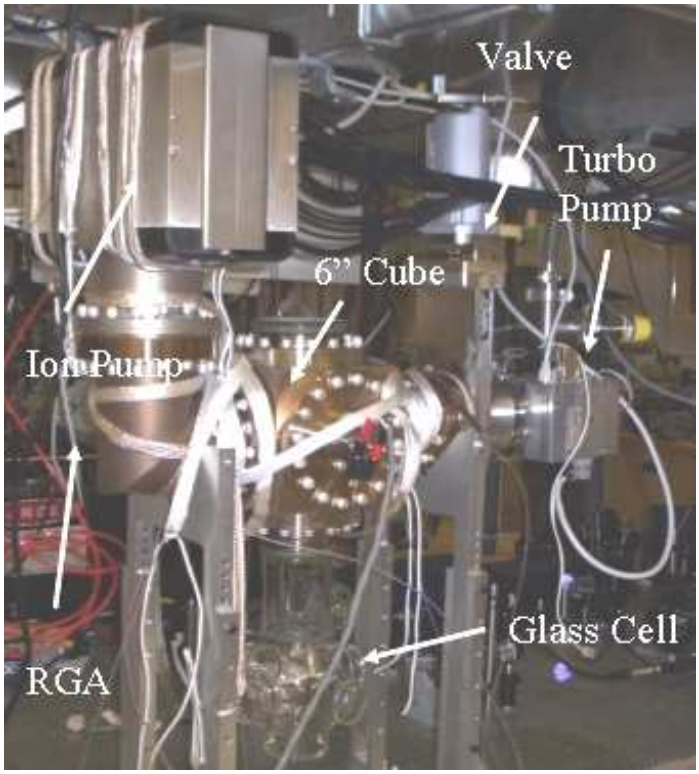

Figure 5.1: Completed vacuum system with major components labeled

the titanium anodes. Basically an ion pump works by creating an electron discharge (Penning tubes) in the middle of the pump. Particles that enter into the pump are ionized and accelerated to towards the anode. When they collide with the anode, which is made of titanium, they sputter titanium onto the walls of the pump. This acts as a getter for certain particles, specifically H_2, N_2 and O_2. Certain ion pumps have holes in the anode, which allow ions to travel through and bury themselves into the pump wall. There, they are shielded by the anode from further ion bombardment. This prevents the pump from occasionally releasing large amounts of gas, specifically argon. Certain hole patterns in the anode are thought to be better than others. The Duniway pattern is a spiral, thus the name galaxy. We decided against a titanium sublimation pump due to cost and to see if we could get the required pressures without one. The completed vacuum system is shown in figure 5.1.

5.1.1 Air Bake

One of the major sources of outgassing once in the ultra-high vacuum regime is hydrogen from stainless steel. This effect can be mitigated by adding an oxide layer on the outside of the steel by baking the steel in air[25]. Therefore, we baked our stainless steel vacuum components in a glass oven which goes up to 560^o and then turns off. Once the parts went through this process they turned a golden yellow colour.

5.1.2 Cleaning Vacuum Parts

When constructing an ultra-high vacuum system it is important that all surfaces are completely clean of oils. Oils have a very high vapour pressure and the pressure of the entire system will be limited by this pressure until the oil is completely gone. This may take months or even years. Therefore, good vacuum procedure requires one to wear gloves when touching the vacuum parts at all times. Before the parts are to go into vacuum they need to be cleaned of all oils and contaminants. The process we used is as follows:

1. Put on lab coats, hair nets and 3 layers of gloves.
2. Clean all parts with hot water and alconox to remove very heavy contaminant rinsing with hot water.
3. Dry and rinse once more with hot water to remove all the alconox.
4. Rinse with deionized water.
5. Rinse with trichloroethylene, acetone and methanol (in that order) inside a fume hood.
6. Rinse with deionized water. Let dry.

5.1.3 Assembly

Once all the components were cleaned, it was time to assemble them together. All of the components were attached using the conflat flange (CF) system. In this system the seal between two components is a metal to metal seal. The two components both have a sharp edge around the rim which lines up. A copper gasket is placed between the two knife edges. Bolts provide the pressure between the two sides. As the bolts are tightened the knife edges 'dig' into the copper. This provides a seal which is good for at least 10^{-12} Torr. When tightening a flange based on this system there is a specific process.

1. Hand tighten all the bolts so that the gasket is firmly in place between the two components.
2. Using a wrench turn one of the bolts a few times.
3. Repeat with the bolt opposite to the one just tightened.
4. Continue this pattern around the circle of bolts.
5. Continue the whole process until the bolts cannot be further tightened (using human power).

The system was assembled and the turbo pump was turned on. Figure 5.2 shows the RGA scan that was performed at this time. The scan shows that a lot of the cleaning solvent was left over in the chamber.

5.1.4 Vacuum Bake

To increase the rate at which outgassing occurs and to therefore deplete sources of high pressure in the vacuum system it is necessary to heat the vacuum system. This process is known as baking the vacuum system. For our bake we used the following process:

1. Bake with turbo pump to 200°C for approximately 1 week.

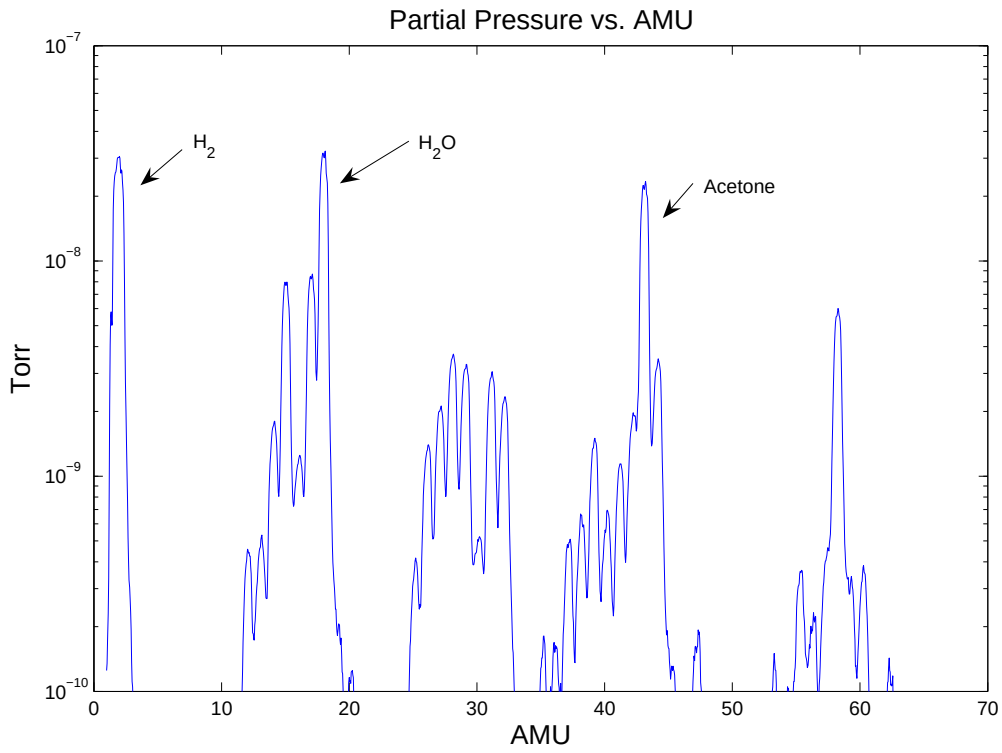

Figure 5.2: RGA scan after turbo pump was turned on for the first time

2. Cool down and close the valve to the system.

3. Turn on the ion pump and let run for 1 day.

4. Bake again at 200°C until pressure rises then starts to fall.

5. Cool back down.

.

Ideally you would like to bake as hot as possible, however, we were limited to 200° by certain components of the system, specifically the valve. To bake we wrapped the system with heater tape from Omega, attached 7 thermocouples to the system and covered the entire system in at least 2 layers of aluminum foil. We attached the heater tapes to variac power supplies and slowly turned the voltage up. The main concern was to prevent spatial temperature gradients in the glass.

After the first week we cooled the system down, turned on the ion pump and took the RGA scan shown in figure 5.3. This is a huge improvement over the first time the system was pumped down (figure 5.2). Next, we started heating up for the ion pump bake. The idea is that outgassing will increase with the increase in temperature. However, this will start to deplete the sources and the outgassing will eventually decrease. This will be evident from the system pressure which is proportional to the ion pump current. This is not what took place, as will be described in the next section.

5.1.5 Leak Testing

During the ion pump bake it became evident that the pressure was not starting to decrease. In fact, the pressure became so high that the ion pump turned itself off (a precautionary measure built into the system). We cooled down the system to room temperature and took the RGA scan seen in figure 5.4. The system had increased in pressure since figure 5.3. Also, argon, which was not there before, was around in large quantities. Argon is the noble gas in the largest quantities in the earth's atmosphere ($\sim 1\%$[26]). Noble gases are very hard to pump as they are unreactive and therefore,

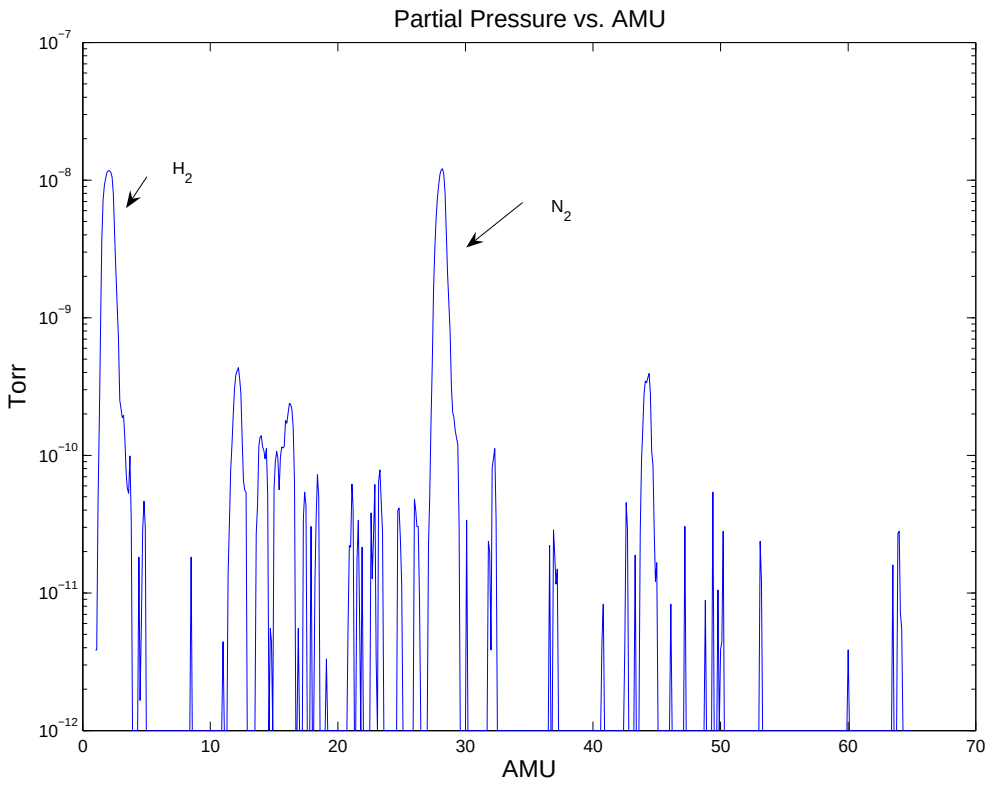

Figure 5.3: RGA scan after ion pump was turned on for the first time

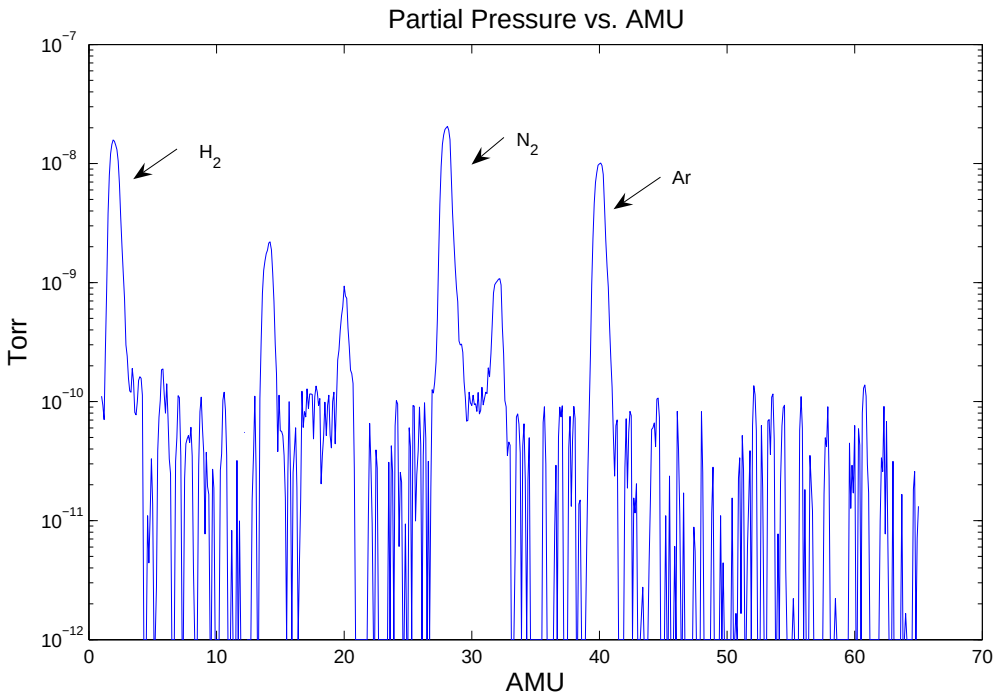

Figure 5.4: RGA scan after system developed a leak

argon leaking into the system would become a significant source of high pressure. Evidence of argon in the system lead us to believe that a leak was possible.

To test for leaks you spray some gas around the system and look for that gas in the system. If an RGA is not available, you look at the system pressure (from ion pump current). The pressure will go down since the gas is plugging the leak, then the pressure will go back up once all the gas has made it through. To leak test the system we used methanol as the indicator. A scan of methanol versus time in the system is shown in figure 5.5. Since the methanol spiked this is definitive proof the system had a leak. It turned out the system had two leaks. One in a crack in the top window and another in the electrical feedthrough for the dispenser current. Both were sealed with a sealant compound from Kurt Lesker. This worked very well and eventually such a low pressure was achieved that the ion pump current indicator is not sensitive enough to give a reading. The RGA scan for the system on April 10, 2006 is shown in figure 5.6. As is seen in the figure, H_2 is the dominant source of pressure in the

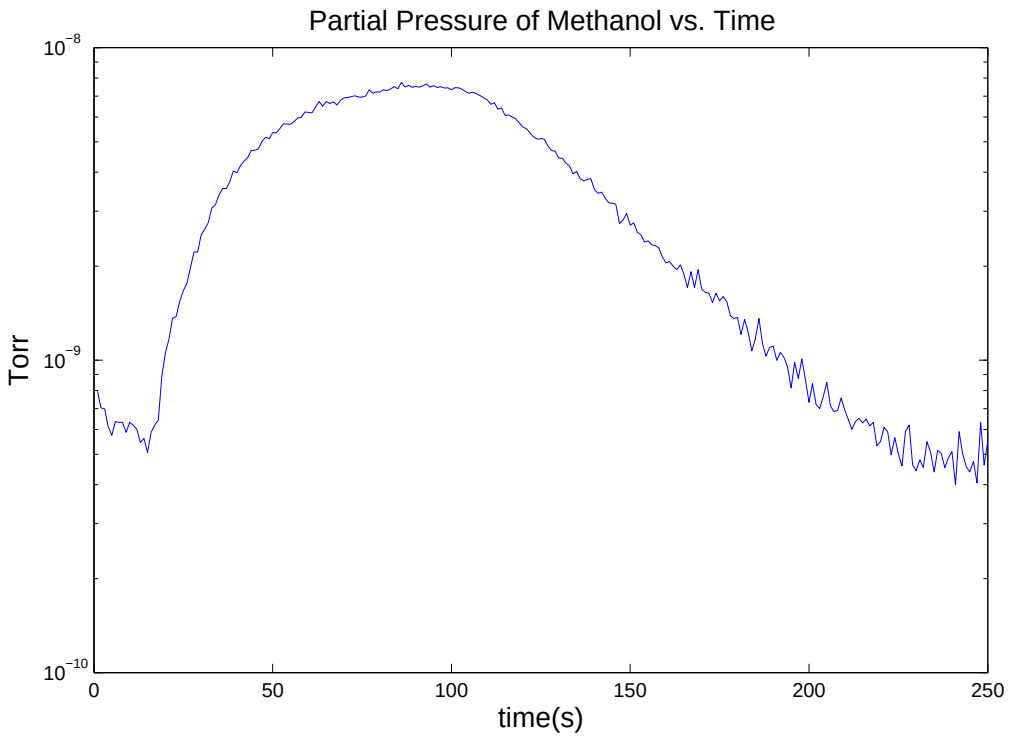

Figure 5.5: RGA scan of methanol during leak testing

system. This is likely from the stainless steel walls. This is a positive reading because it means we have limited all possible preventable sources of outgassing. The only way to further increase the system pressure would be to add a titanium sublimation pump, which is very good at pumping H_2.

5.2 A Magneto-Optical Trap Pressure Gauge

With the vacuum system assembled the next stage was to setup the elements required to create a magneto-optical trap in the system. The theory for a magneto-optical trap (MOT) was outlined in section 2.3, however, there are several ways to implement a MOT. For instance, in the main system a single beam is expanded and then split into 6 beams. These beams form the 3 sets of counter-propagating beams. An easier setup, which we used for this test system, is to enlarge and split into three beams. These beams are sent through the system and then reflected back off of mirrors to

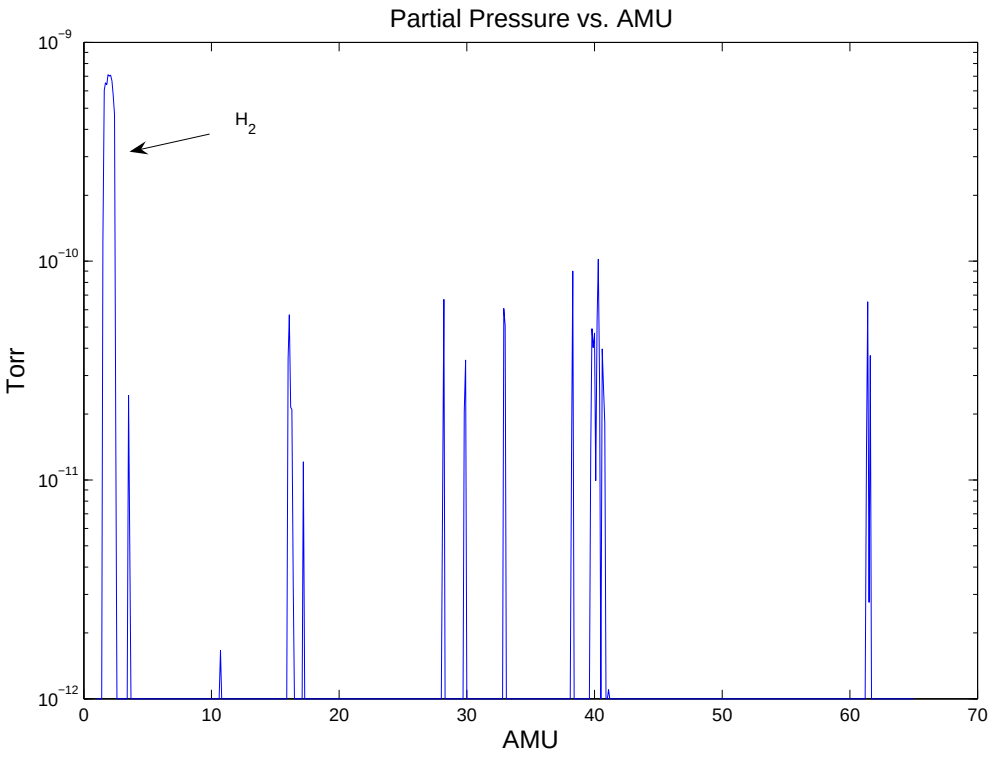

Figure 5.6: April 10, 2006 RGA scan

create counter-propagation. This is known as a retro-reflecting mot. The plan was to send two sets of counter-propagating beams through the sides of the glass cell and the final set in the vertical direction from the bottom of the cell through the window in the top of the vacuum system. In the following, the setup of the system will be discussed, followed by the alignment of the MOT. Then the imaging system will be discussed and MOT lifetime results will be presented. These lifetime measurements will become the basis of the MOT pressure gauge.

5.2.1 Setup

An overview of the optics for the system is shown in figure 5.7. A flipper mirror is used to divert the beam out of the tapered amplifier from the main experiment into the test system. Then, the beam is sent through a 5x beam expander to create a beam size of ~ 1 cm diameter beam. Note that instead of going straight through the expander the beam is reflected off several mirrors and goes through two apertures. The purpose of this is for system alignment. Two apertures can be shrunk down to two points to create a line. If the beam is centered on these apertures then they set alignment for the beam. For example, if one of the mirrors is bumped, then the alignment procedure is to close down the apertures and re-center the beam. Apertures are used extensively through the system to enable quick re-alignment of the system after the first alignment.

After going through the beam expander the beam is split into three. Beam splitters are used to split the beam into two paths (this process is done twice). Beam splitters transmit horizonally polarized light and reflect at 90° vertically polarized light. To control the amount of light transmitted and reflected half wave plates are placed before both beam splitters. Half way plates rotate linearly polarized light and offer a method to control the power balance. Before going into the cell the linearly polarized light passes through a quarter-wave plate, which creates circularly polarized light. This is necessary for the formation of a MOT (see section 2.3). The beam passes through the cell and then through another quarter-wave plate. This makes the polarization go back to linear. The light then reflects back into the cell, going through the quarter-

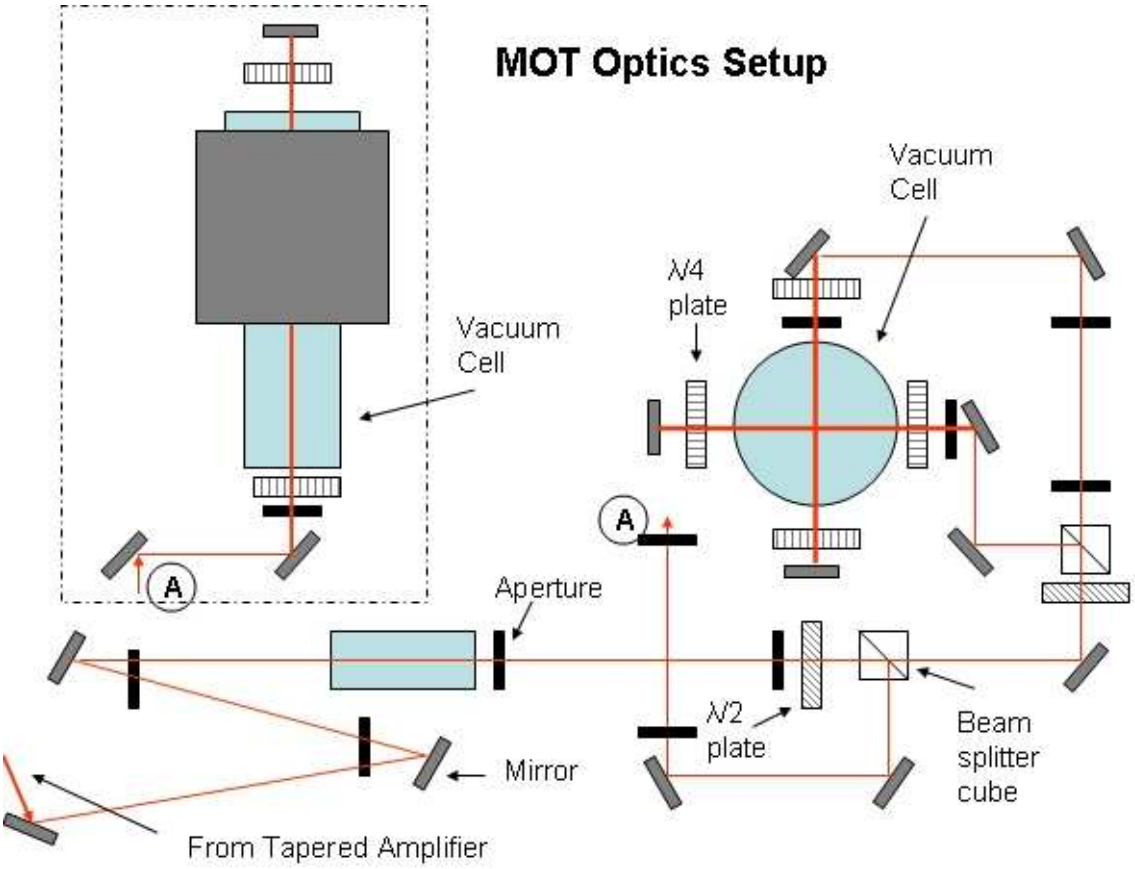

Figure 5.7: Overview of the MOT optics

wave plate and becoming circularly polarized again. The light will be polarized in the same circular direction, except the propagation vector is reversed. This creates the proper σ^+, σ^- required to create the MOT.

Another required element of the MOT setup is a pair of magnetic field coils. The common rule of thumb for the required gradient when building a MOT is 15 G/cm. A simple calculation shows that the gradient along the axis at the center between two coils with equal but opposite currents is:

$$\frac{\partial B}{\partial x} = -\frac{3NI\mu_0 R^2}{2}\left(\frac{2d}{(R^2+d^2)^{5/2}}\right) \tag{5.1}$$

where R is the coil radius, 2d is the distance separating the two coils, I is the current and N is the number of turns. For coils of 10 cm diameter and separated by 10 cm, the gradient is 15 G/cm if the current in the coils is 5.6 A and the number

of turns in 100. Beldon Type 8076 20 gauge wire was wrapped on an $\sim$ 11 cm pipe. Every 25 turns 5 minute epoxy was applied to the wire to keep the coil shape. After 100 turns the coil was let to dry and then removed from the pipe.

5.2.2 Alignment

For the MOT to work correctly the beams have to cross in the vacuum system and this crossing has to correspond to the magnetic field minimum. A rough alignment was completed with the setup of the mirrors. The mirrors for the two sets of beams in the plane of the table were set at equal heights. The difficult alignment is the beam coming up from the bottom. To complete this alignment the chamber was flooded with rubidium. With enough rubidium the beams can be seen on an inexpensive CCD camera. The beams were made as thin as possible by closing the aperture directly after the beam expander. Once the beams were aligned the magnetic field was aligned by moving the coils.

5.2.3 Imaging System

The final element for measuring the MOT lifetime is to measure the power of the fluorescence from the MOT. This requires setting up an imaging system to focus the MOT light onto a photo-diode. To do this a telescope was created with two f=10cm lenses set 20 cm apart. This focuses an image 10 cm from one lens 10 cm from the other lens with no magnification.

5.2.4 Observing a MOT

A MOT was first observed on February 7, 2006. The MOT was observed from the fluorescence, which was captured by a CCD camera positioned outside the vacuum cell. A typical MOT image is illustrated in figure 5.8. However, the lifetime of this MOT was very poor and it only appeared in a small detuning range. Three methods were used to improve the MOT.

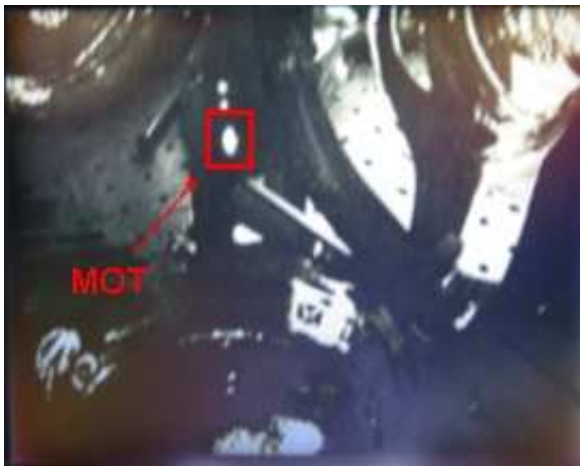

Figure 5.8: Fluorescence image of the MOT

- Power Balance: For a proper MOT, the power in all three beams should be equal.
- Laser Power: If the laser power is too high the MOT will only work at large detunings because at low detunings the atoms are still saturated. Also, when the MOT is formed large densities are created. This causes 2-body collisions in the MOT, which limits the lifetime below the loss caused by background collisions.
- Retro Reflection: A subtle point of the retro reflection MOT is that the beam has to go through the atoms and then reflect back again. If the beam is perfectly aligned then there is a power hole in the middle since some of the power was absorbed by the trapped atoms as the beam made its first pass. Because of this, a slightly out of alignment retro reflected beam works slightly better.

5.3 Results

Lifetime measurements were made once the MOT was aligned and working correctly. A good laser power was found to correspond to $\sim$ 975 mA of current in the tapered amplifier and $\sim$ 4.5 A of coil current.

5.3.1 Data Collection

The signal from the photodiode was put through a 1MΩ resistor, which was fed into a non-inverting op amp circuit with gain of ~ 10. The output of the op amp was sent to a LabJack analog to digital converter, which was connected to a laptop running Windows XP. The data was streamed from the LabJack at a rate of 1000 samples per second. Because of high frequency noise on the signal either from the photodiode or the amplifier circuit, the collected data was run through a 50 point running mean filter in MatLab. A set of wrapper classes was written in C++ for communicating with the LabJack.

5.3.2 Lifetime Measurements

The lifetime was extracted from the fluorescence power collected by a photodiode. An example fit is shown in figure 5.9. Using this technique a value of 34.7±2.6s was obtained for a coil current of 4.65(2) A, a detuning of 11.1497(1) MHz and a TA current of 981(1) mA. The pressure is determined by the equation

$$P = \frac{1}{\tau \sigma_{Rb-x}} \left(\frac{m_x kT}{3} \right)^{1/2}, \tag{5.2}$$

where x is the most dominant background element. This equation is a combination of the ideal gas law and equation 2.12. From the RGA scan we know that the background gas is dominated by H_2. The collisional cross section is calculated to be $295 \times 10^{-20} m^2$[27]. Using this value, and a value of 295K for the temperature the pressure is calculated to be $1.1(1) \times 10^{-10}$ Torr.

There are two main questions regarding this result. The first question addresses the validity of the τ obtained from the fits as it relates to the lifetime due to collisions with background atoms. As was mentioned in section 2.3, the majority of the MOT loss is from collisions in the MOT related to the density. Then, at what point do background losses dominate and at what point to two-body losses dominate? The second question has to do with the error in the fluorescence values from the LabJack.

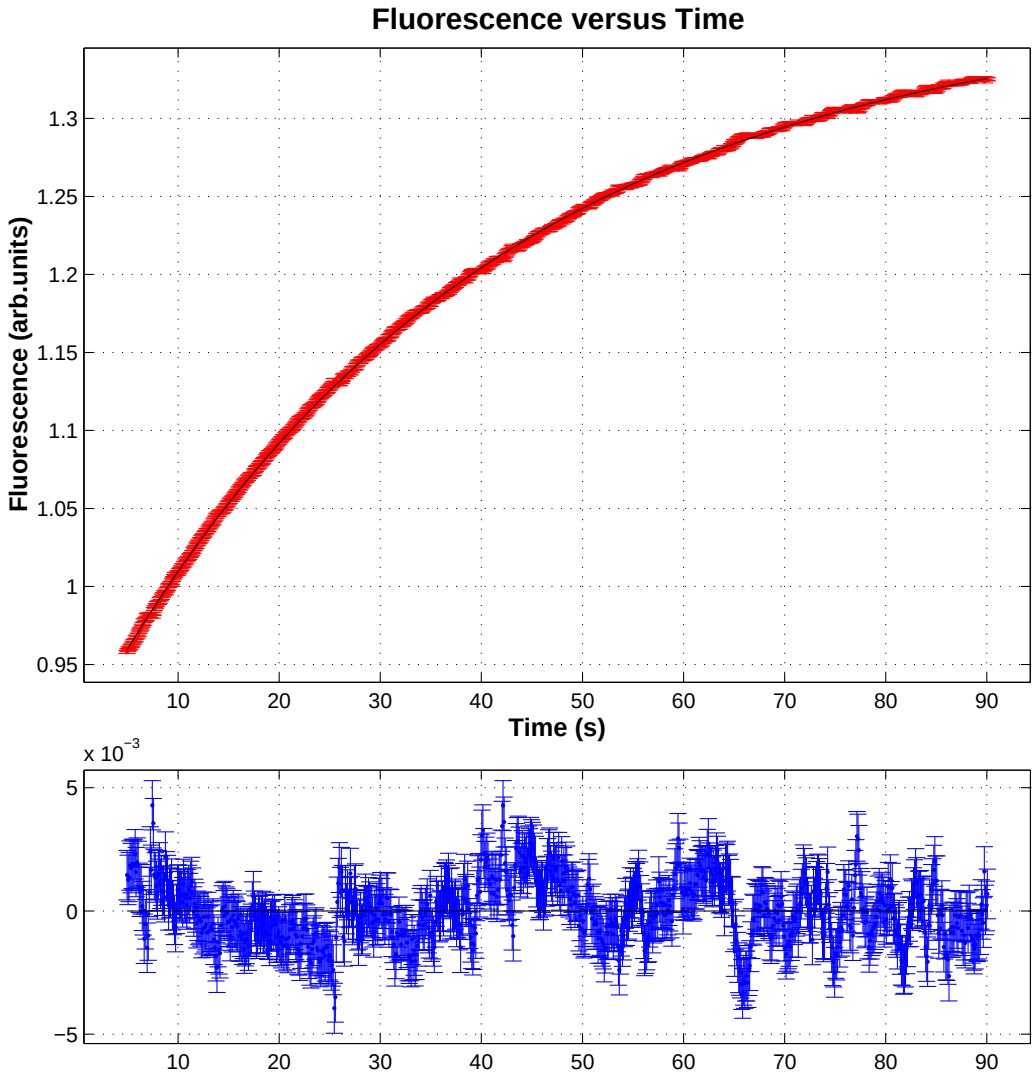

Figure 5.9: An example of a lifetime fit to MOT fluorescence data. Error in the signal was estimated to be 0.001 based on noise in the detector when there was no MOT signal. The distribution of the residual appears to be random, which indicates no serious systematic error.

5.3.3 Atom Number

The amount of fluorescence is a measure of the number of atoms in the MOT. Other factors contribute as well, including the beam intensity and the detuning. The equation that links all these parameters is[15]

$$P = \frac{hc}{\lambda}\frac{\Omega}{4\pi}N\frac{\Gamma}{2}\frac{I/I_0}{1+I/I_0+(2\Delta/\Gamma)^2}, \tag{5.3}$$

where Ω is the solid angle subtended by the detector, Γ is the line width of the transition, Δ is the detuning and I_0 is the saturation intensity. We would just like an order of magnitude for the number of atoms in the trap. The values for I_0, Γ, λ and Ω are 1.6 mW/cm^2, 6 MHz, 780 nm [7] and 0.125 respectively. From the Thorlabs catalogue the photodiode we are using (DET110) has a spectral response of $\sim$ 0.5 A/W. It generates a signal of $\sim$ 0.5 V into a 1MΩ impedance. This corresponds to roughly 1μW of power when I $\sim$ 6.5 mW/cm^2 and a detuning of 9 MHz. Putting this power into the formula we get an atom number of approximately 10^8 atoms.

5.3.4 Lifetime versus Detuning

The lifetime was measured as the detuning was changed from 6MHz to 20MHz. A plot of lifetime versus detuning is shown in figure 5.10.

This is very interesting because the lifetime was expected to be constant. What likely is the case is that for lower values of detuning the trap is becoming more dilute. This is causing the time constant to be a better estimate of the lifetime due to background loss versus the lifetime due to two body collisions inside the MOT.

5.3.5 Lifetime versus Light Intensity

One of the things that was noticed when initially aligning the MOT is that high light intensity can significantly decrease the lifetime. Also, the MOT will only form for larger detunings. For this measurement we changed the input light power while also changing the detuning to maximize the fluorescence signal from the MOT. The result

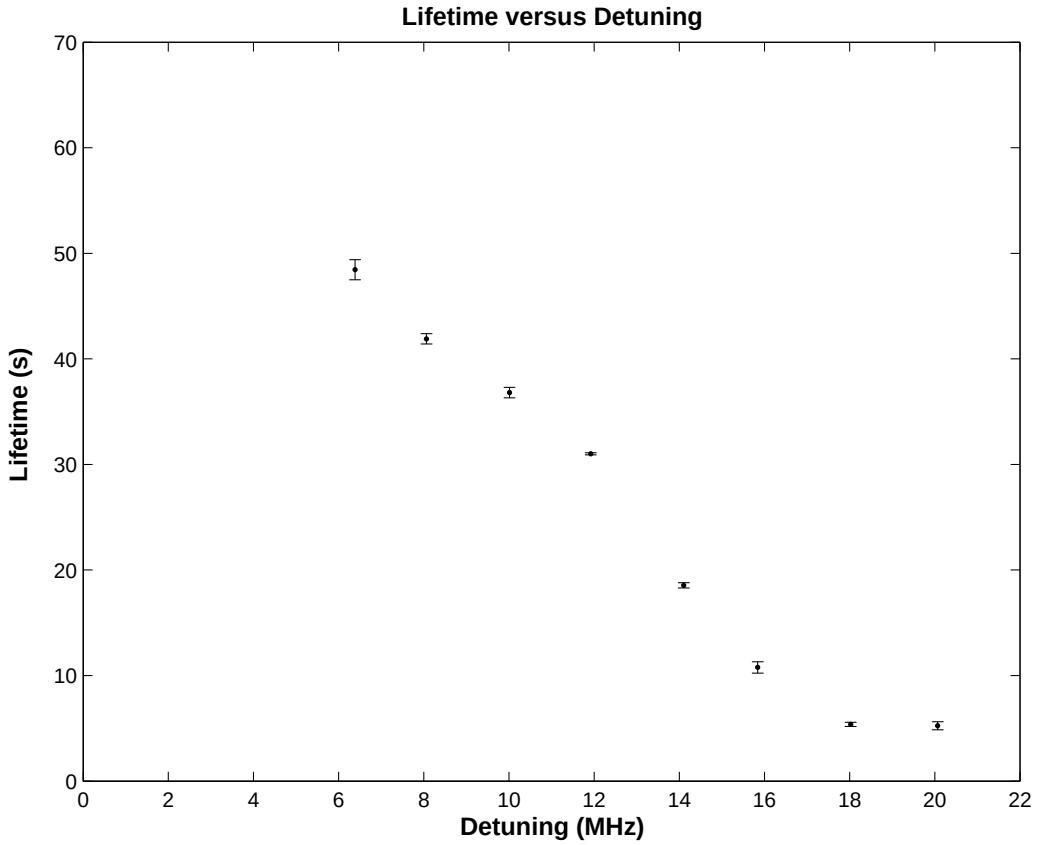

Figure 5.10: Lifetime versus Detuning plot. Tapered amplifier current was held constant at 981(1) mA ($\sim$ 34 mW) and the coil current at 4.65(3) A.

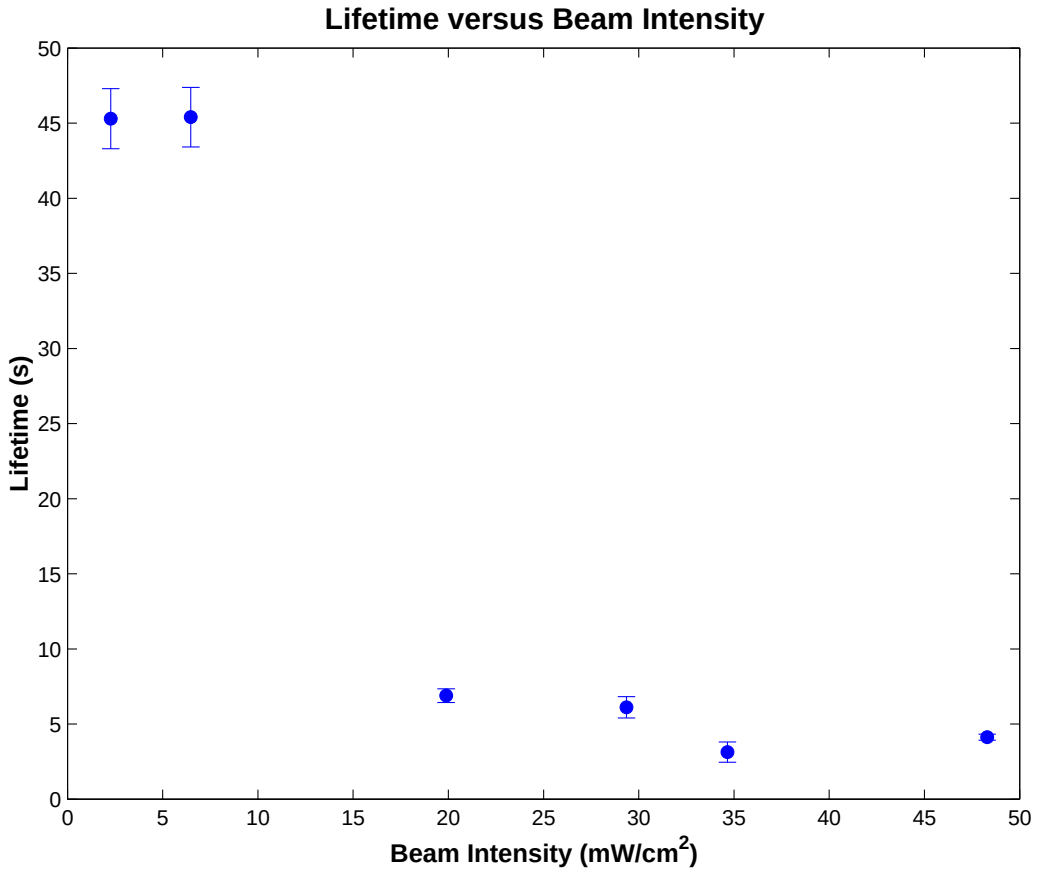

Figure 5.11: Lifetime versus Light Intensity. The first two points were at a detuning of $\sim$ 9 MHz, then the next two points were held at detunings of 21.2 MHz then the next points were held at detunings of 26.4 MHz and 31 MHz respectively. Detunings were selected on a rough maximization of the photodiode output. The coil current was held steady at 4.65(3) A.

can be seen in figure 5.11.

5.3.6 Lifetime versus Pressure

To make this measurement the turbo-pump and the roughing pump were shut off. Because there is a leak in the valve this slowly causes the pressure in the system to rise. If we plot lifetime versus pressure we get figure 5.12. This is fit to equation 5.2. The data for this is not very good because the pressure is read off the ion pump, which is not very accurate. Also, the pressure was changing quickly in the system. The χ^2 for the fit was 46 for 6 DOF. The fit was to the equation $\tau = a_1/P + a_2$ (refer

to equation 5.2) where $a_1 = 5.3(4)$ s/Torr and $a_2 = 4.9(2)$ s.

5.3.7 Lifetime versus Dispenser

The dispenser was turned on at 4.5 A for 20 minutes and then shut off. Lifetime measurements were made a certain times after the dispenser had been turned off to measure how quickly the ^{87}Rb is pumped out of the system. This is shown in figure 5.13. Even though the dispenser has an adverse effect on the lifetime, indicating a slightly higher system pressure, we can't use the previous result (figure 5.12) to give the exact rise in system pressure since the lifetime is still better than 15 s. What this graph does show is that the dispenser does have an effect on the lifetime of the MOT, which is to be expected since we purposely add vapour to the chamber. However, what this result also shows is that the pressure only slowly improves. When the rubidium vapour is effecting the lifetime we cannot accurately gauge the 'real' pressure of the system. However, we need Rb to make the MOT. This result shows that we cannot take background pressure until at least a couple of hours after the dispenser has been run.

5.4 Conclusions

There were many strong accomplishments in this section of the project. A vacuum system was designed, ordered, assembled and fixed from leaks. All the MOT optics were assembled and aligned and an imaging system was constructed. Finally, a MOT was created and lifetime data was extracted. However, we must not forget the bigger purpose of this project is to provide an accurate measure of the background pressure. Yet, much of the data works against this principle in that the MOT lifetime, which we were to use to extract pressure, changes based on many factors. Besides the measured pressure, which was our goal, we saw lifetime dependences on detuning and light intensity. This is not good because it affects our ability to say the lifetime accurately reflects the pressure. It is likely that the correlation between all these dependences has to do with the density of the MOT, which increases the likelihood of

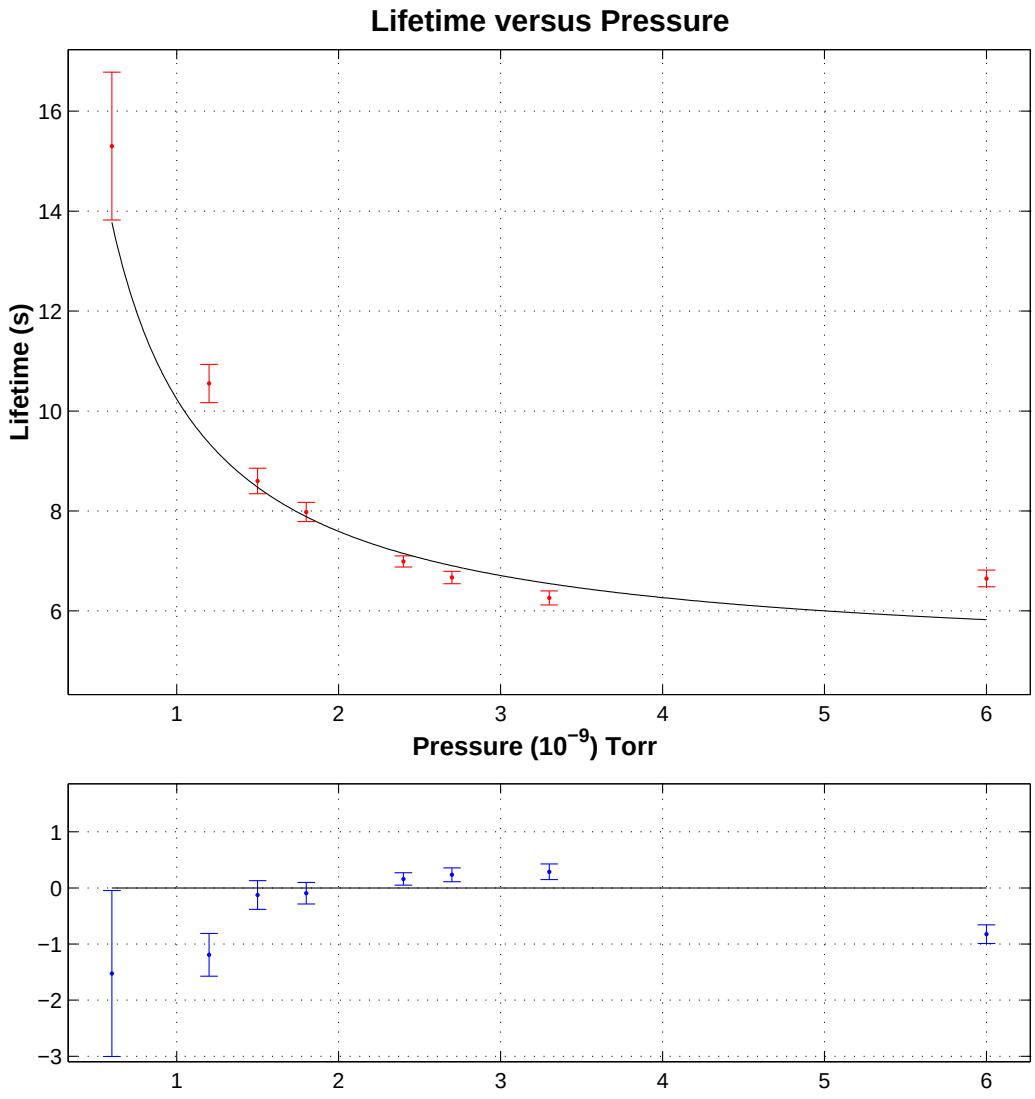

Figure 5.12: Lifetime versus Pressure plot. Tapered amplifier current was held constant at 981(1) mA ($\sim$ 34 mW) and the coil current at 4.65(3) A.

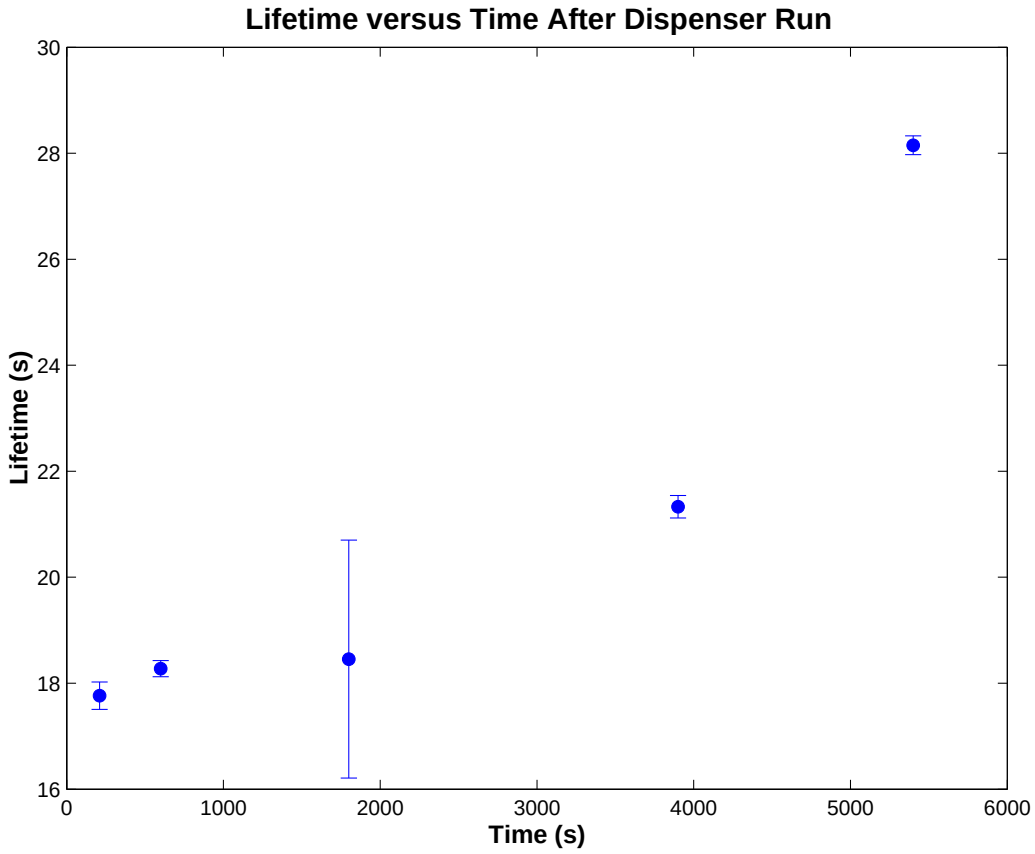

Figure 5.13: Lifetime versus Time after the Dispenser is Turned Off. Tapered amplifier current was held constant at 981(1) mA ($\sim$ 34 mW) and the coil current at 4.65(3) A.

2 body collisional loss from inside the MOT. These effects on lifetime do not reflect the pressure of the system correctly.

Therefore, to accurately measure the lifetime as it pertains to the system pressure we need to make sure we make measurements in the regime of the most dilute MOT possible. This means a low light intensity, small detuning and a long time since the dispenser was last night.

Chapter 6

Conclusions

There is still a lot of work to do with both of these projects. For the high frequency sources the clear future direction is testing both these sources by actually evaporating cold atoms. This will lead to a lot of information such as if the sources can provide the required stability and if further amplification is needed.

A lot of work is remaining for the stack project. The stack needs to be constructed with all the wire connections and a chip. When the stack system is under construction the high frequency connections need to be tested with the new high frequency sources. Once the stack is assembled, the test vacuum system needs to be opened and the stack set inside. After baking the vacuum properties of the stack will be tested using the MOT technique demonstrated in this thesis. There is still some work with the evaluation of these techniques as we have to determine how best to control the system parameters to measure only background collisional loss.

While the new stack is being vacuum tested, a new potassium 40 dispenser needs to be constructed. Once the ^{40}K dispenser is constructed and the stack successfully vacuum tested they will be combined and placed in the main experiment. At this point the projects developed in this thesis will then truly become tools to manipulate cold atoms.

Despite all the future work that needs to be done, a lot was accomplished with this thesis. These accomplishments include constructing two high frequency sources, designing a new stack, building a vacuum system, creating a MOT and observing a

lifetime versus pressure signal.

Bibliography

[1] Brian DeMarco. *Quantum Behavior of an Atomic Fermi Gas.* PhD thesis, Univeristy of Colorado, 2001.

[2] Daniel A. Steck. Rubidium 87 d line data. Los Alamos National Labs Theoretical Division, 2003.

[3] MDC Vacuum, www.mdcvacuum.com.

[4] J. Reichel, W. Hansel, P. Hommelhoff, and T. W. Hansch. Applications of integrated magnetic microtraps. *Applied Physics B*, 72(1), 2001.

[5] J. Reichel, W. Hansel, and T. W. Hansch. Atomic micromanipulation with magnetic surface traps. *Physical Review Letters*, 83, 1999.

[6] S. Aubin, S. Myrskog, M.H.T. Extavour, L.J. LeBlanc, D. McKay, A. Stummer, and J.H. Thywissen. Rapid sympathetic cooling to fermi degeneracy on a chip. cond-mat/0512518, to appear in Nature Physics, 2006.

[7] Harold J. Metcalf and Peter van der Straten. *Laser Cooling and Trapping.* Springer, 1999.

[8] Pathria. *Statistical Mechanics.* Butterworth-Heinemann, 1996.

[9] Joseph Thywissen, 2006. Personal Communication.

[10] John Weiner, Vanderlei S. Bagnato, Sergio Zilio, and Paul S. Julienne. Experiments and theory in cold and ultracold collisions. *Reviews of Modern Physics*, 71, January 1999.

[11] E.L. Raab, M Prentiss, Alex Cable, Steven Chu, and D.E. Pritchard. Trapping of neutral sodium atoms with radiation pressure. *Physical Review Letters*, 59(23), 1987.

[12] P.A. Willems and K.G. Libbrecht. Creating long-lived neutral-atom traps in a cyrogenic environment. *Physical Review A*, 51(2), 1995.

[13] Benjamin Lev. *Magnetic Microtraps for Cavity QED, Bose-Einstein Condensates, and Atom Optics.* PhD thesis, California Institute of Technology, 2006.

[14] C. Monroe, W. Swann, H. Robinson, and C. Wieman. Very cold trapped atoms in a vapor cell. *Physical Review Letters*, 65(13), 1990.

[15] D. Rapol, Umakant, Ajay Wasan, and Vasant Natarajan. Loading of a rb magneto-optic trap from a getter source. *Physical Review A*, 64, 2001.

[16] Kirstine Berg-Sorensen. Kinetics for evaporative cooling of a trapped gas. *Physical Review A*, 55(2), 1997.

[17] Ian Leroux. Manipulation of ultra-cold atoms using radio-frequency and microwave radiation. Master's thesis, University of Toronto, 2005.

[18] Alan Stummer, 2005. Personal Communication.

[19] Shengwang Du, Matthew B. Squires, Yutaka Imai, Leslie Czaia, R.A. Saravanan, Victor Brigh, Jakob Reichel, T.W. Hansch, and Dana Anderson. Atom-chip bose-einstein condensation in a portable vacuum cell. *Physical Review A*, 70.

[20] Marcius T. Extavour. Design and construction of magnetic elements for trapping and transport of cold neutral atoms. Master's thesis, University of Toronto, 2004.

[21] G. Thieme. Mass spectrometer investigation of gas emission from plastics. Published in Vacuum, date unknown.

[22] K.F. Poole and M.M. Michaelis. Hialvac and teflon outgassing under ultra-high vacuum conditions. *Vacuum*, 30(10), 1980.

[23] Charles A. Grubbs. Anodizing of aluminum. *Metal Finishing*, 100, 2002.

[24] Kevin Moore, 2006. Personal Communication.

[25] John F. O'Hanlon. *A User's Guide to Vacuum Technology*. Wiley, 2003.

[26] nssdc.gsdc.nasa.gov/planetary/earthfact.html.

[27] S. Bali, K.M. O'Hara, M.E. Gehm, S.R. Grenade, and J.E. Thomas. Quantum diffractive background gas collisions in atom-trap heating and loss. *Physical Review A*, 60(1), 1999.

Appendix A

Microwave Spectra

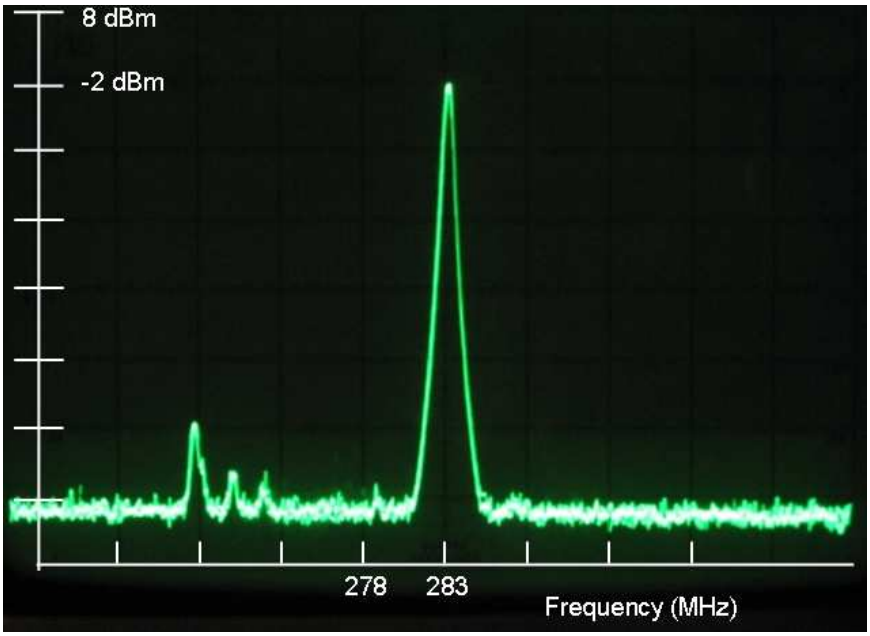

Figure A.1: Spectrum from just after the AD9858 outputting 283 MHz

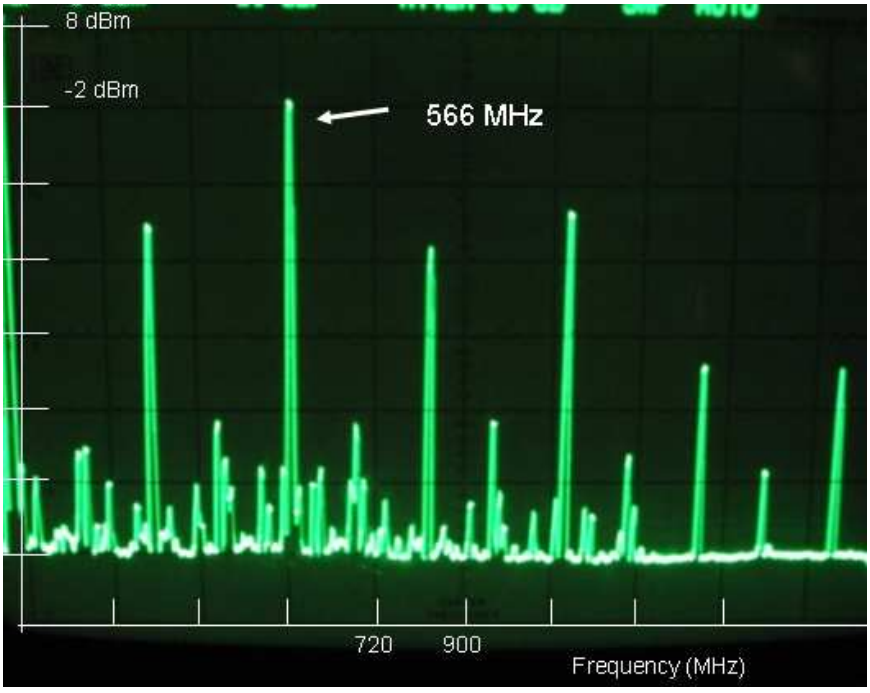

Figure A.2: Spectrum from location A1 in the 6.8 GHz system

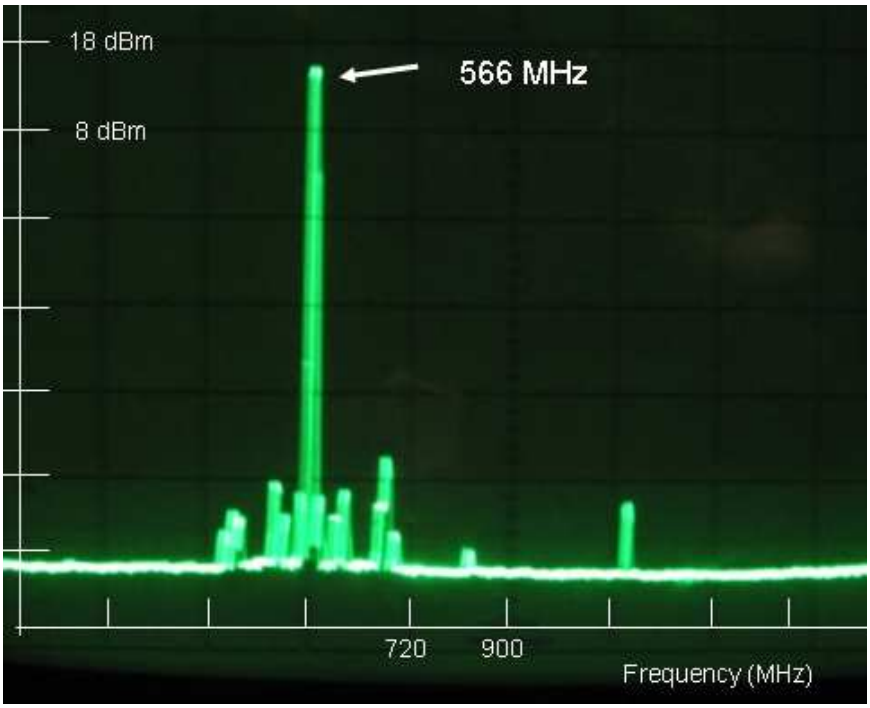

Figure A.3: Spectrum from location A2 in the 6.8 GHz system

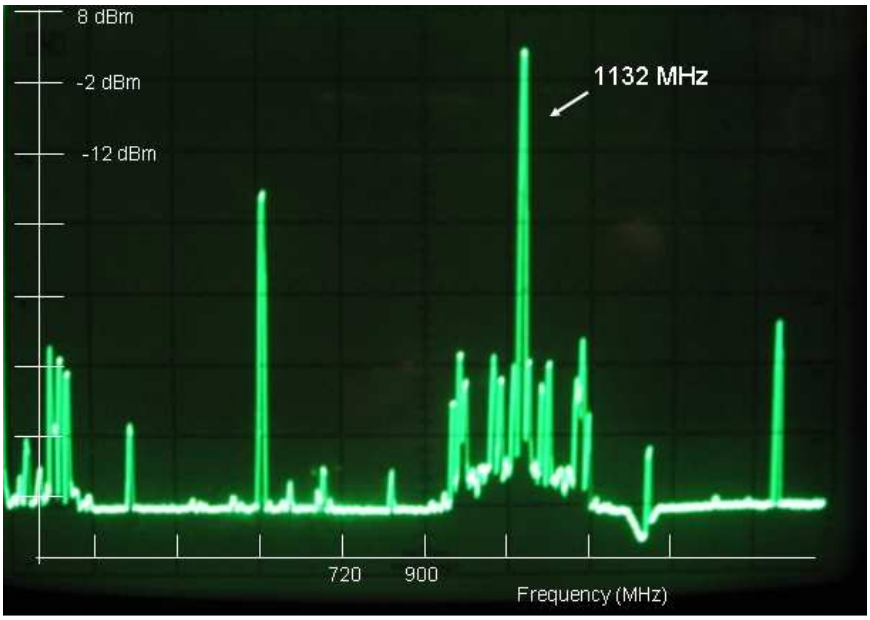

Figure A.4: Spectrum from location B1 in the 6.8 GHz system

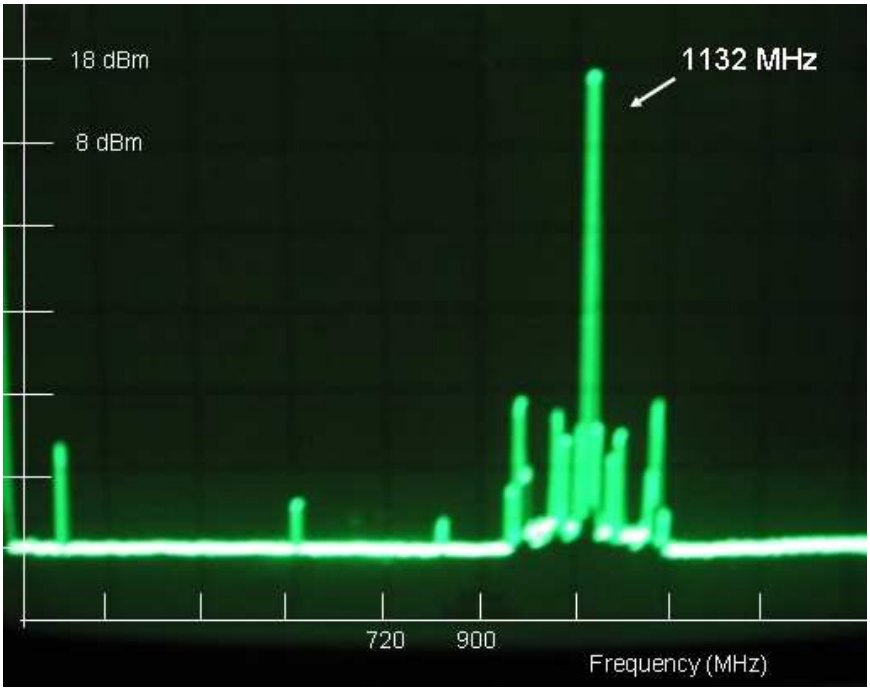

Figure A.5: Spectrum from location B2 in the 6.8 GHz system

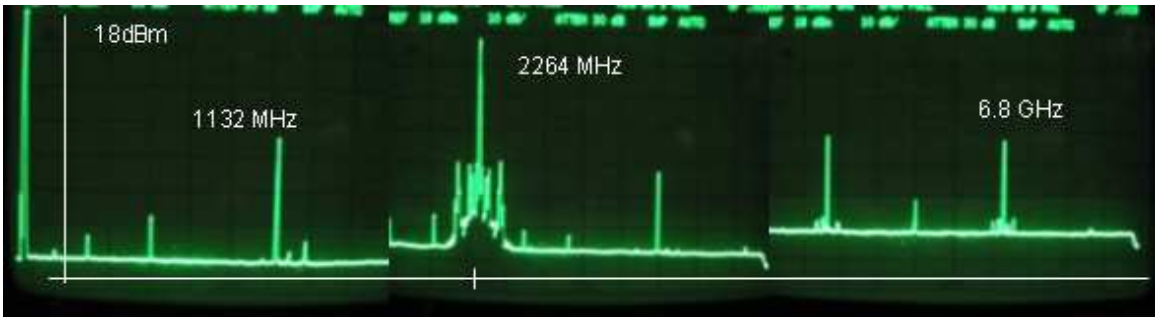

Figure A.6: Spectrum from location C1 in the 6.8 GHz system

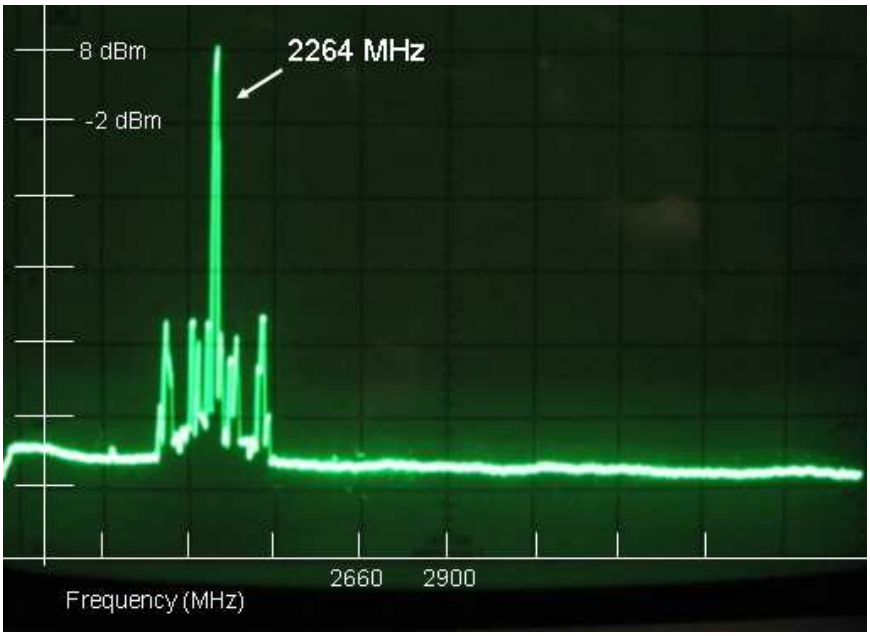

Figure A.7: Spectrum from location C2 in the 6.8 GHz system

Figure A.8: Spectrum from the output of the 6.8 GHz system (not filtered)

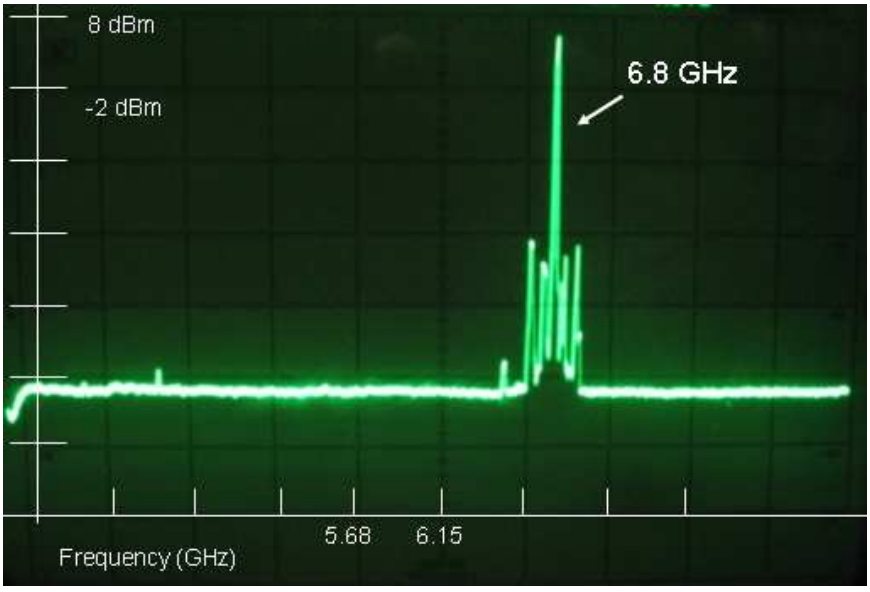

Figure A.9: Spectrum from the output of the 6.8 GHz system (filtered). The main harmonics from the previous figure have been filtered out, however, there is some noise at the base of the 6.8 GHz peak. Some investigation is needed to determine this source, but since this is a logarithmic scale, this noise is a factor of 1000 times less power than the main signal.

Appendix B

CAD Drawings

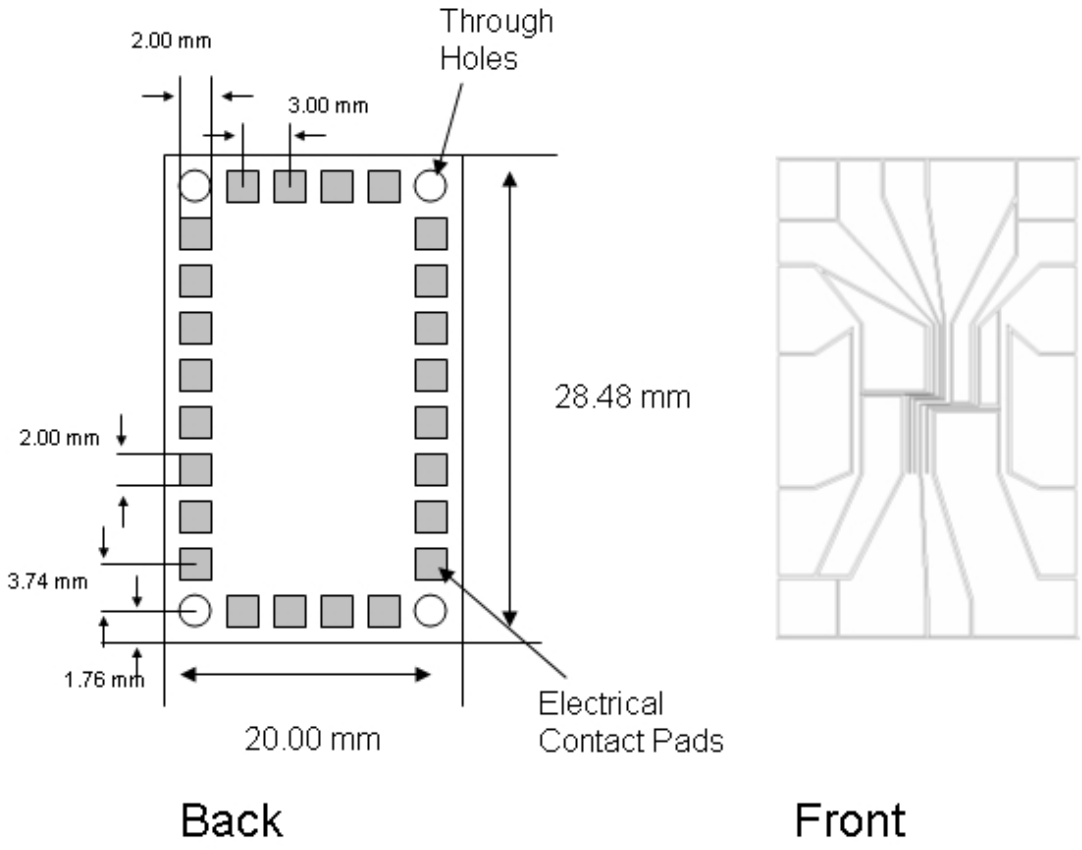

Figure B.1: Schematic of the new chip for the Thywissen lab experiment

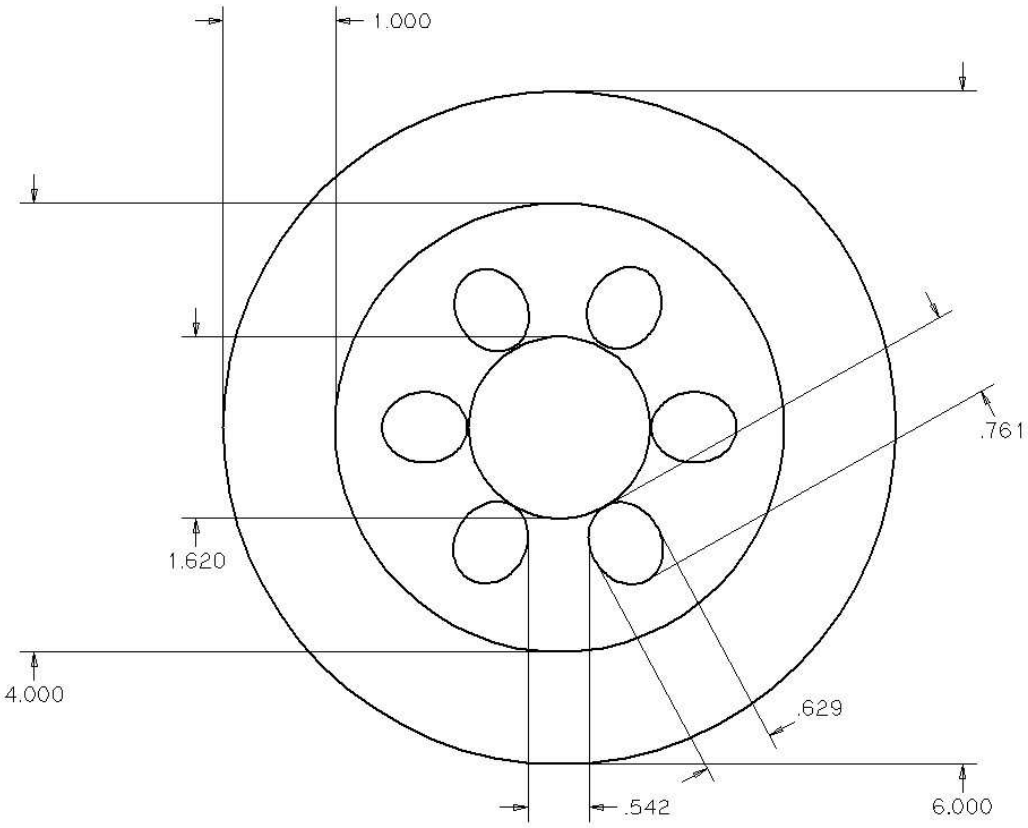

Figure B.2: Schematic of multiport flange

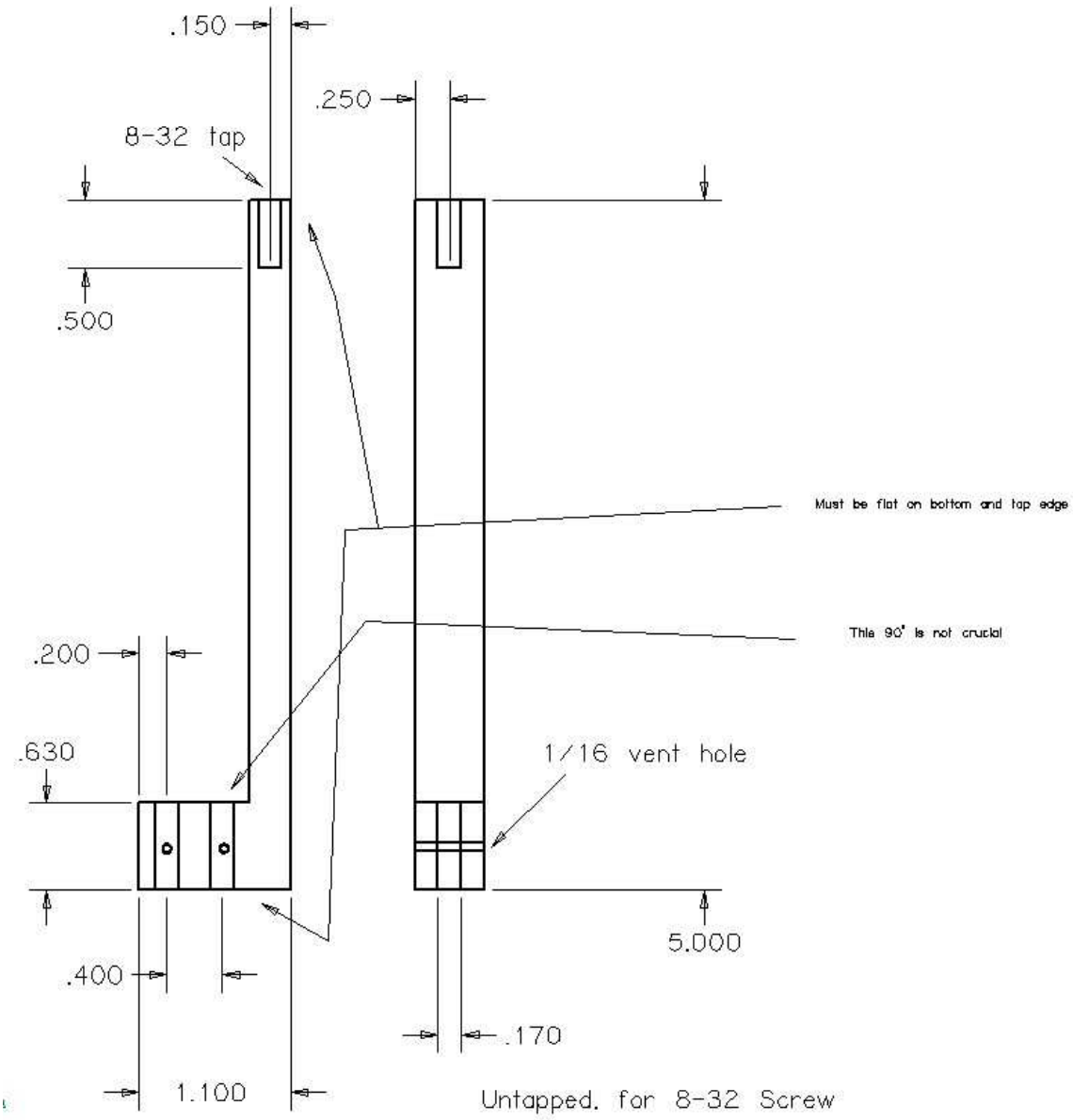

Figure B.3: CAD drawing of stack 'leg'

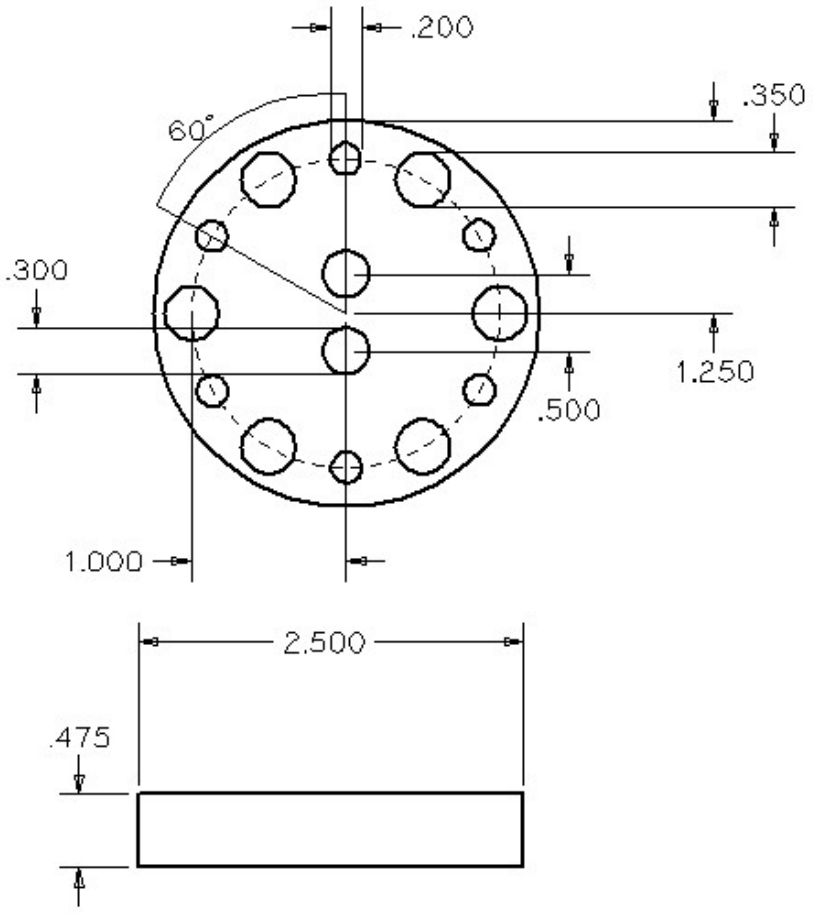

Figure B.4: CAD drawing of stack reducer

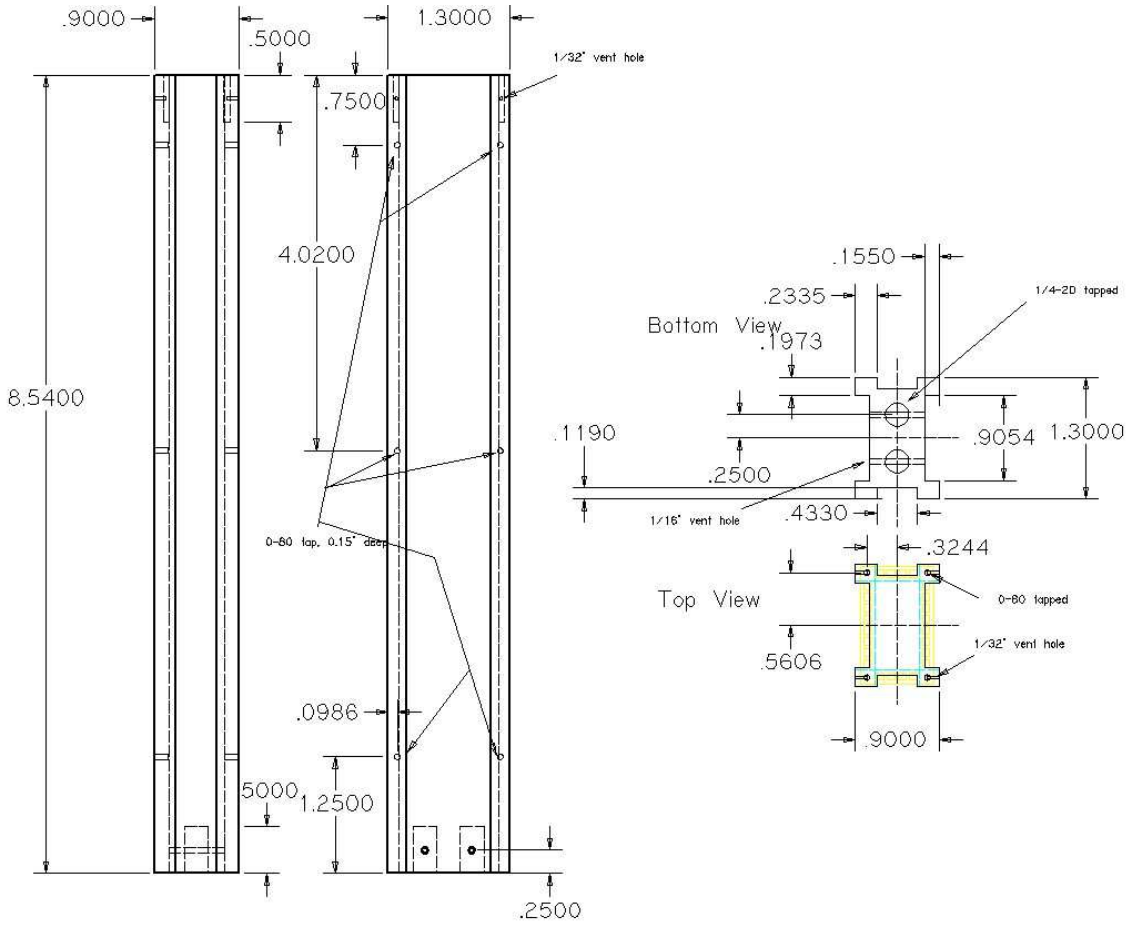

Figure B.5: CAD drawing of stack body

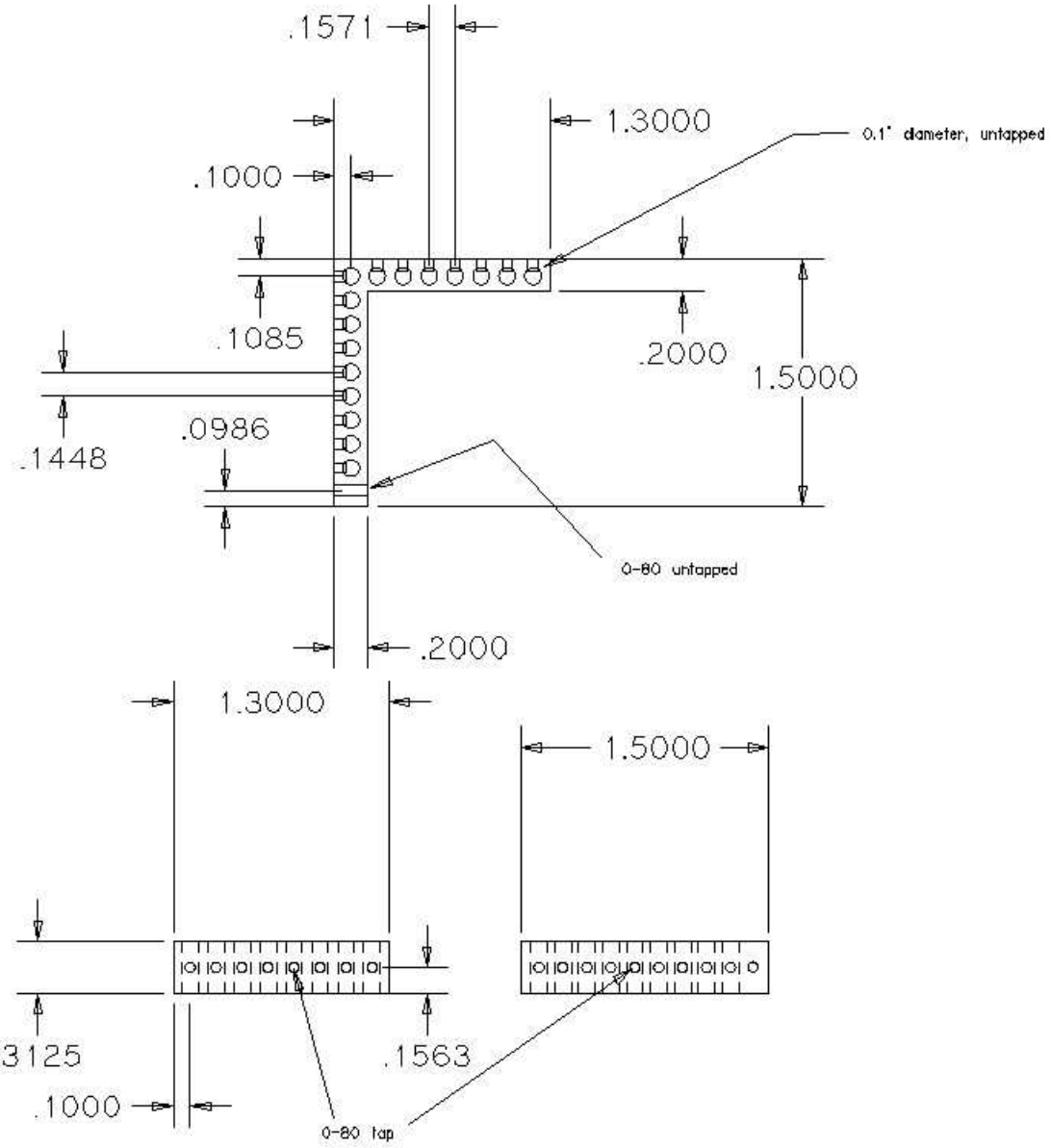

Figure B.6: CAD drawing of stack bottom wire guide

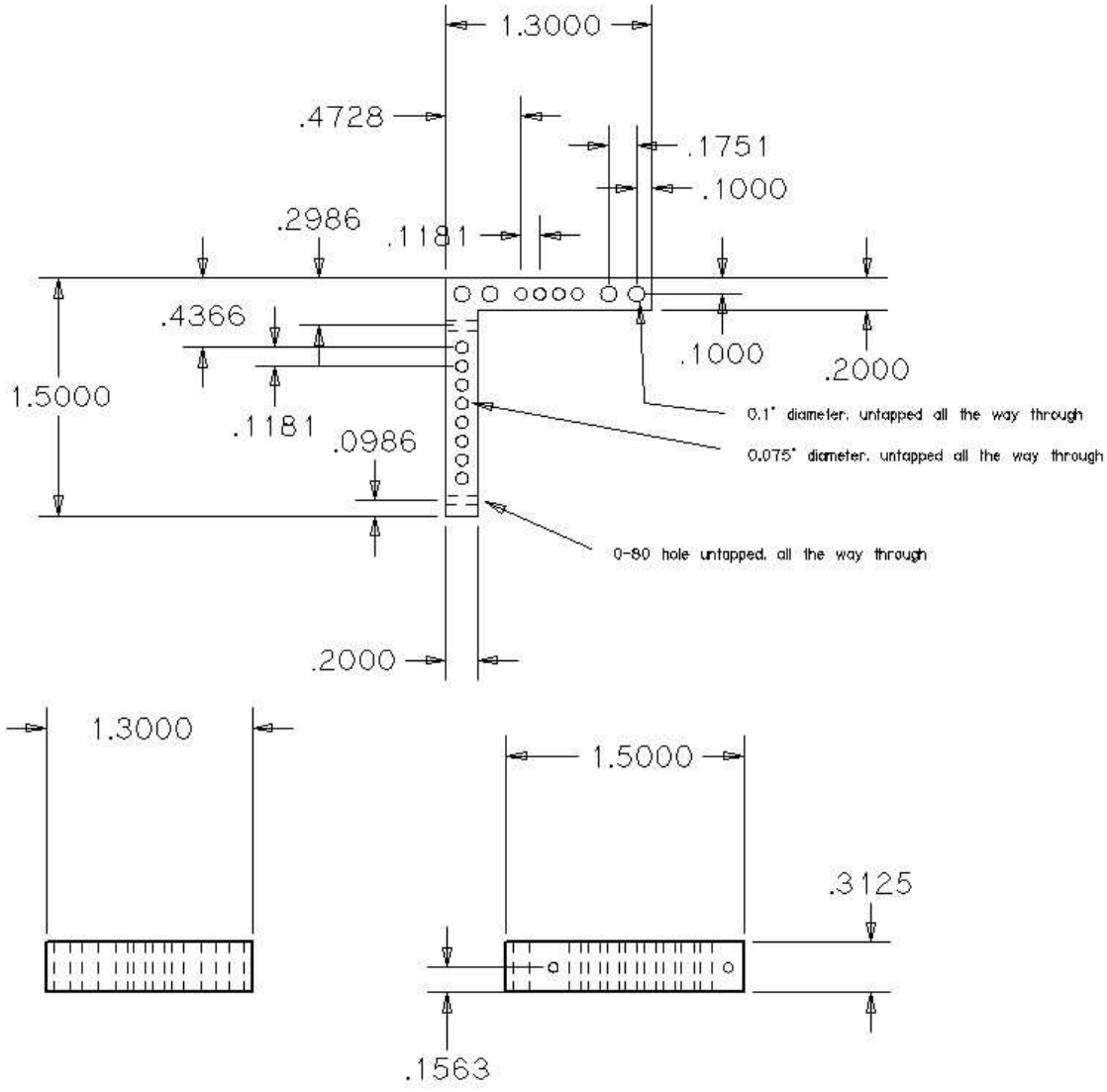

Figure B.7: CAD drawing of stack middle wire guide

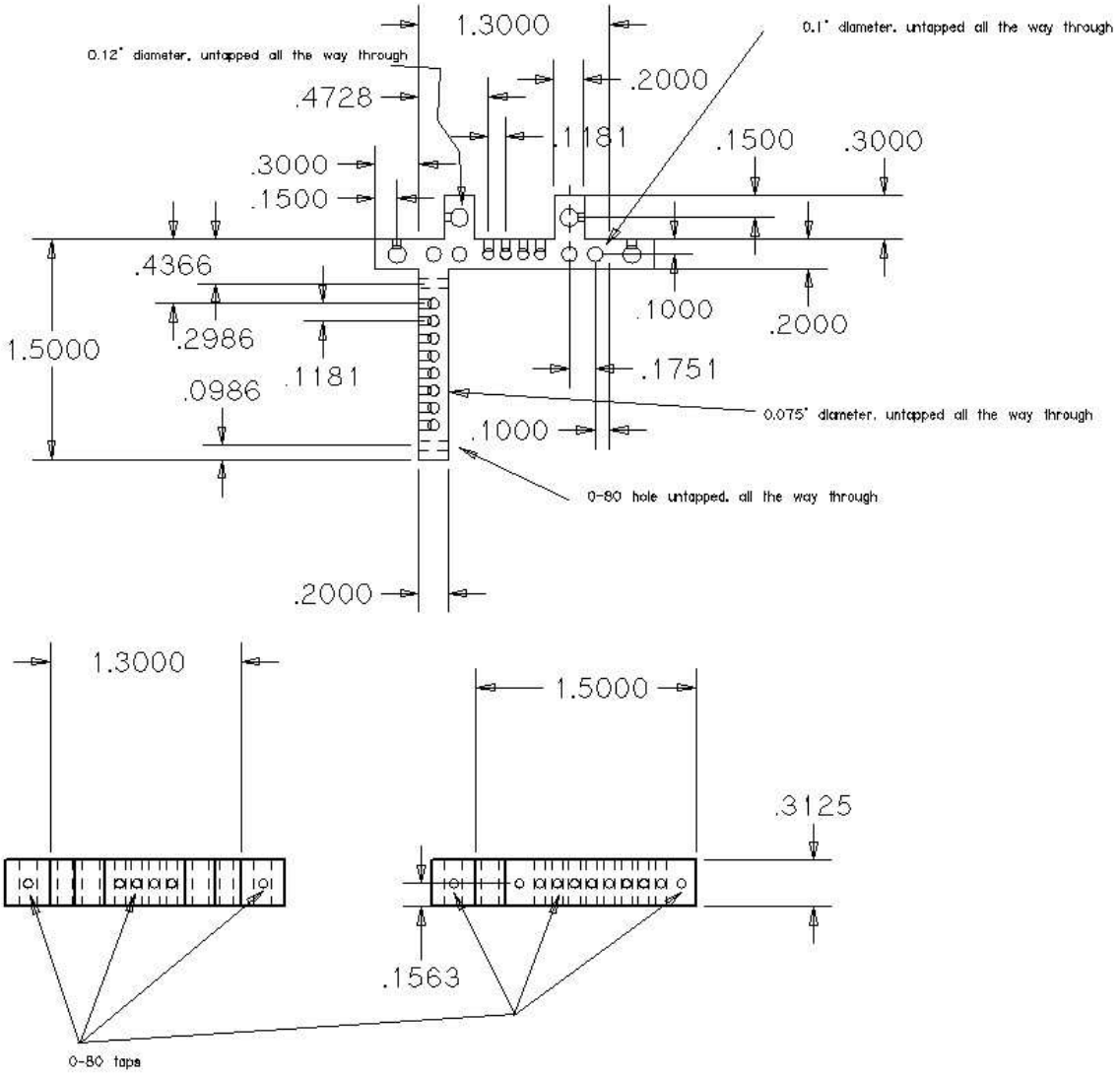

Figure B.8: CAD drawing of stack top wire guide

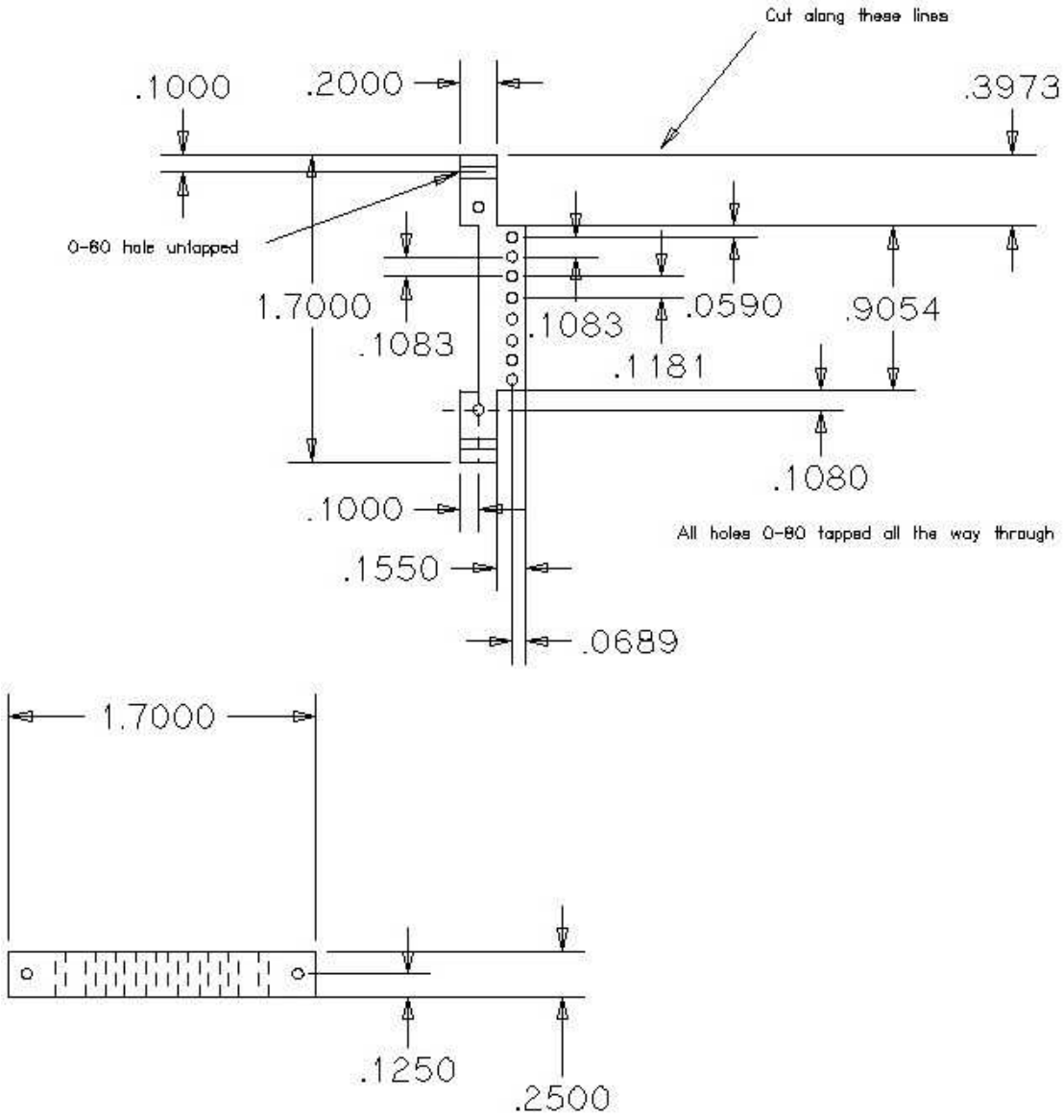

Figure B.9: CAD drawing of chip connector (part 1)

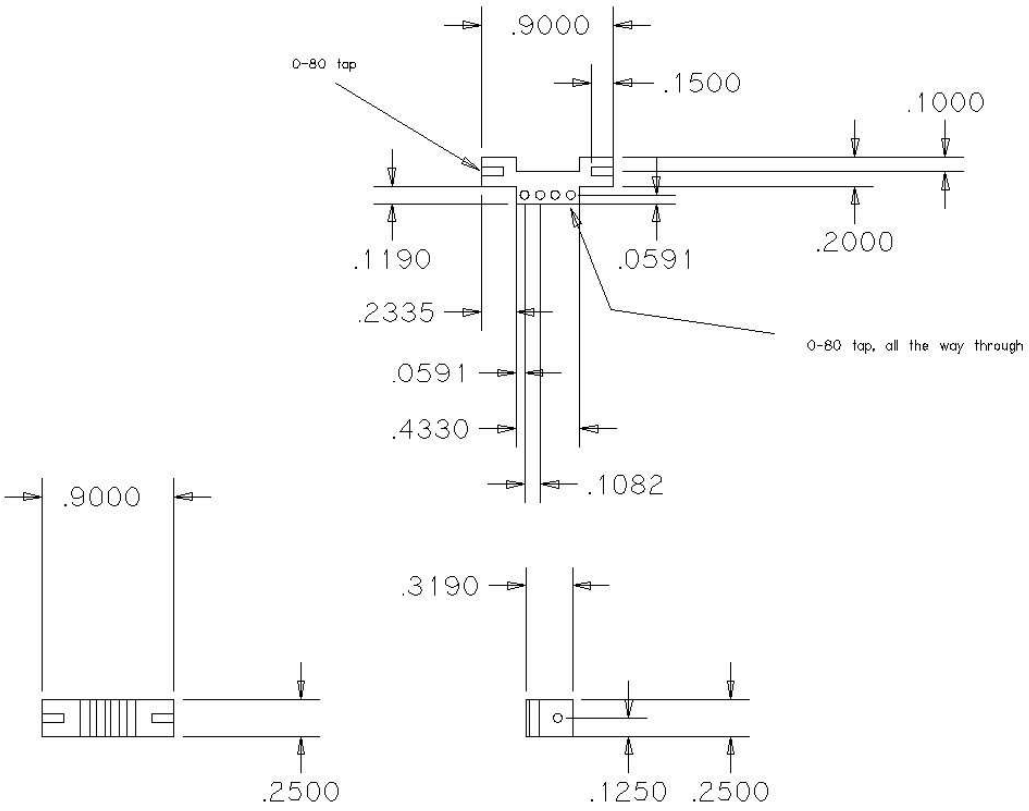

Figure B.10: CAD drawing of chip connector (part 2)

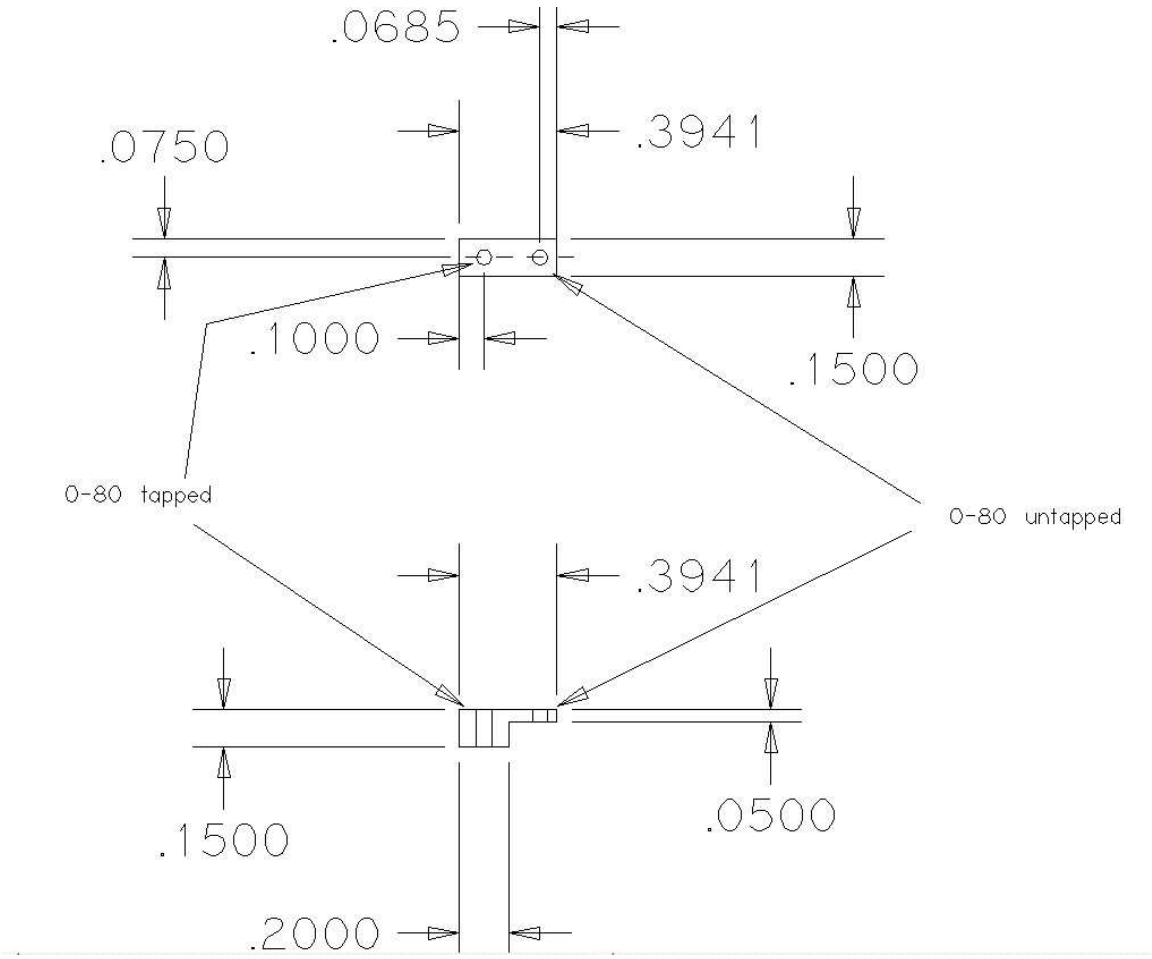

Figure B.11: CAD drawing of washer